Journal of Medicinal Chemistry

Article

pubs.acs.org/jmc

3-Oxo-hexahydro-1*H*-isoindole-4-carboxylic Acid as a Drug Chiral Bicyclic Scaffold: Structure-Based Design and Preparation of Conformationally Constrained Covalent and Noncovalent Prolyl Oligopeptidase Inhibitors

Gaëlle Mariaule, Stéphane De Cesco, Francesco Airaghi, Jerry Kurian, Paolo Schiavini, Sylvain Rocheleau, Igor Huskić, Karine Auclair, Anthony Mittermaier, and Nicolas Moitessier*

Department of Chemistry, McGill University, 801 Sherbrooke Street West, Montréal, Québec H3A 0B8, Canada

Supporting Information

ABSTRACT: Bicyclic chiral scaffolds are privileged motifs in medicinal chemistry. Over the years, we have reported covalent bicyclic prolyl oligopeptidase inhibitors that were highly selective for POP over a number of homologous proteins. Herein, we wish to report the structure-based design and synthesis of a novel class of POP inhibitors based on hexahydroisoindoles. A docking study guided the selection of structures for synthesis. The stereochemistry, decoration, and position within the molecule of the bicyclic scaffolds were assessed virtually. Following the synthesis of the best candidates, *in vitro* assays revealed that one member of this chemical series was more active than any of our previous inhibitors with a K_i of 1.0 nM. Additional assays also showed that the scaffold of this potent inhibitor, in contrast to one of our previously reported chemical series, is highly metabolically stable, despite the foreseen potential sites of metabolism. Interestingly, computer docking calculations accurately predicted the optimal features of the inhibitors.

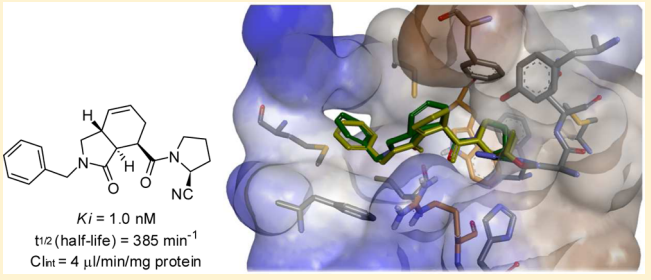

INTRODUCTION

Proline oligopeptidase (POP, sometimes referred to as PREP) is a serine protease which cleaves short peptides at the α-carbonyl of a proline residue. POP was discovered in the mid-seventies, and its high concentration in the central nervous system (CNS) immediately drew attention.[1−3] Early studies attributed POP protease activity to the cleavage of neuropeptides and peptide hormones, and inhibition of this activity was first investigated with the discovery of the reversible covalent inhibitor Cbz-Pro-Prolinal (**1**) over 30 years ago (Figure 1).[4] However, after significant medicinal chemistry efforts and clinical trials, this interest reached a plateau with covalent inhibitors such as JTP-4819 (**2**)[5,6] and KYP-2047 (**4**),[7,8] and noncovalent inhibitors such as S-17092 (**3**).[9] More recently, the potential of such inhibitors in the treatment of Alzheimer's disease and Parkinson's disease has spurred a second boost in the development of POP inhibitors.[1−3,10] Among the important findings are the establishment of an ability to disrupt protein−protein interactions,[11] the significant reduction of α-synuclein levels *in vitro* and *in vivo* by POP inhibitors,[12] and the colocation of POP with α-synuclein and β-amyloid.[13] Elevated levels of POP in cancer cells have also been observed, and our previous work has demonstrated that inhibitors can block the POP protease activity in various cancer cell lines.[14,15]

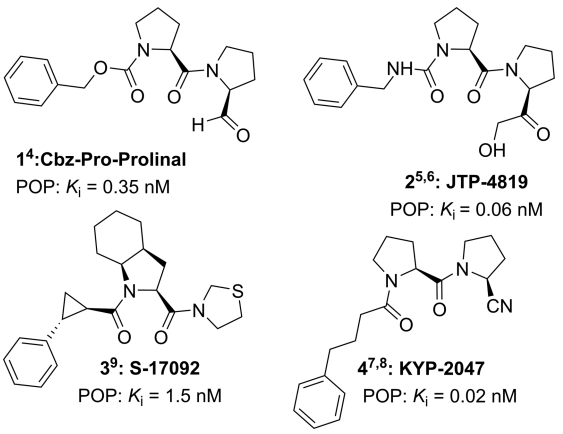

Figure 1. Selected POP inhibitors.

In 2009, we disclosed a series of chiral bicyclic POP inhibitors illustrated with **5** (Figure 2). These covalent inhibitors were found to be cell-permeant and showed enzyme inhibition in the high nanomolar range.[16] Three years later, we

Special Issue: Computational Methods for Medicinal Chemistry

Received: August 21, 2015

DOI: 10.1021/acs.jmedchem.5b01296
J. Med. Chem. XXXX, XXX, XXX−XXX

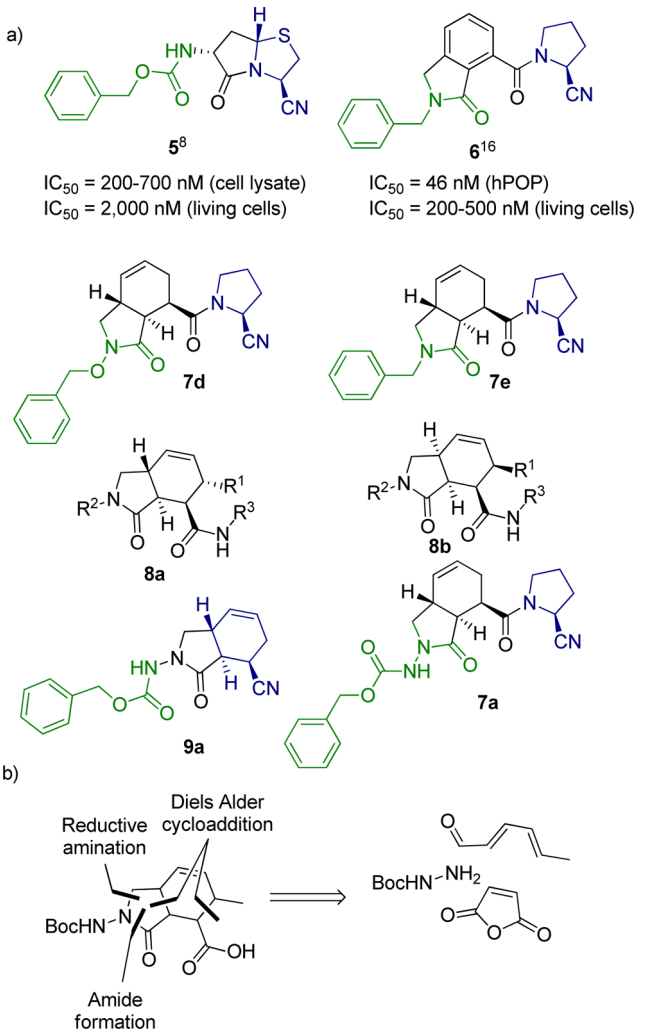

Figure 2. Designed series of potential POP inhibitors.

reported the discovery by virtual screening and docking-guided optimization of a hit molecule, **6**, which turned out to be five times more active than **5**.[15] In addition, we found that the introduction of bicyclic molecular scaffolds improved the metabolic stability of our POP inhibitors.[15] However, some docking studies suggested that the potency of our current lead could be further improved before proceeding with *in vivo* testing, with the potency of **6** being 3 orders of magnitude weaker than the reported potency of **2** or **4**. We wish to report herein our successful efforts in the development of a novel class of POP inhibitors designed from **5** and **6**, and based on a novel bicyclic core.

RESULTS AND DISCUSSION

POP Inhibitors. A large fraction of the reported POP inhibitors are covalent inhibitors, reacting with the catalytic serine (Ser554). Covalent drugs can be extremely effective and profitable pharmaceuticals, yet to date, they have been all but ignored in structure-based drug design campaigns.[17] Until recently, concerns about their potential off-target reactivity and toxicity have often been raised.[18] Lately, however, a significant shift in medicinal chemists' opinion about covalent drugs has been observed, with the advantages of covalent drugs becoming increasingly recognized: these include extremely high potencies, long residence times (slow off-rates), and high levels of specificity.[19−24] Following this trend, **5** and **6** were designed to be covalent inhibitors. However, unlike inhibitors such as **1** and **2** featuring a reactive carbonyl group, we focused our efforts on nitrile derivatives that are significantly less reactive and are likely to provide safer drugs.[25]

Design of Bicyclic Scaffolds. The promising activities of both chiral **5** and achiral scaffold-based **6** led us to design hybrid structures, i.e., chiral (as **5**) structures mimicking **6**. Thus, the aromatic ring was modified (i.e., virtually reduced) leading to several derivatives (**7**) built around scaffolds **8**. Docking studies confirmed that this class of scaffolds was accommodated very nicely in the binding site of POP when the stereochemistry was the one shown in **8a** (Figure 2). We have previously reported a synthetic strategy toward these bicyclic scaffolds (Figure 2b).[26] The use of a bicyclic scaffold is expected to improve the metabolic stability, as we have shown before, as well as the selectivity for POP. In addition, if the fit of these molecules in the POP binding site is optimal, rigidification is expected to reduce the entropic cost associated with ligand binding. Although the shift from achiral to chiral molecules may be perceived as a potential disadvantage, the excellent predicted fit in the binding site led us to further explore this chemical series. In addition, their synthesis is now optimized to the point where no more than two steps are necessary from either readily or commercially available aldehydes.

We have previously reported the synthesis of two diastereomeric members of this novel chemical series with R^1 = Me and R^2 = NH-Boc.[26] The developed synthetic strategy conveniently allows for diversification at R^1, R^2, and R^3.

Structure-Based Design. In order to evaluate the potential activity of **7** and other diversely functionalized and diastereomeric derivatives, we initiated a docking study using our in-house developed program FITTED, which was previously modified to account for covalent inhibition.[15] To date, no crystal structure of the human isoform of POP has been reported (our biological evaluations are carried out on recombinant hPOP), but the high sequence homology of the binding site residues enables the use of porcine POP for docking experiments (97% identity with the human form).[27] Over 20 crystal structures of POP with or without an inhibitor bound are available and were first superposed. The seven most conformationally diverse structures (binding site RMSD greater than 0.2 Å) were identified using our program MATCH-UP and further investigated. As shown in Figure 3, the backbone conformation does not vary significantly between structures, and none of the side-chains adopts a different conformation. Thus, although FITTED can be used in a flexible protein mode, rigid protein docking was expected to provide reliable results. It

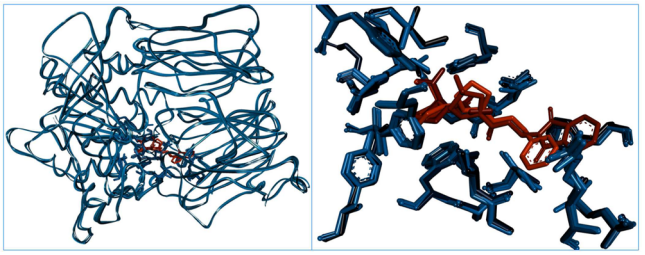

Figure 3. Seven most conformationally different POP crystal structures. Left panel, global fold ribbon diagram; right panel, binding site residues. Co-crystallized inhibitors are shown in orange.

DOI: 10.1021/acs.jmedchem.5b01296
J. Med. Chem. XXXX, XXX, XXX−XXX

is worth noting that adding protein flexibility would have been appropriate if our objective was to design inhibitors structurally very different from the cocrystallized ligands as described in our previous large evaluation study.[28]

Through this docking study, we wished to focus our synthetic efforts toward structures with a high likelihood of being active. Analogues with diverse R^1 and R^2 groups were drawn and docked. The selection of R^1 and R^2 groups considered the synthetic feasibility. Figure 5a shows the binding mode of Cbz-Pro-Pip-CN cocrystallized with POP.[29] As with other cocrystallized ligands, this structure revealed two key hydrogen bonds with Arg643 and Trp595, a covalent bond with Ser554 and hydrophobic interactions with Phe173. Our compounds were docked and compared to this ligand cocrystallized structure (Figure 5b–f).

It was first envisaged that scaffold **8** could be decorated with a (*S*)-cyano-pyrrolidine (R^3 in Figure 2) to provide **7d**, **7e**, and **7a**, as hybrids of **5** and **6**, or alternatively converted into nitrile analogues such as **9a**.

Covalent Inhibition. The physical processes governing the action of covalent bond forming drugs differ fundamentally from those of noncovalent drugs. Covalent drugs inhibit their targets in a two-step fashion (Figure 4).[22] First, they bind

$$E + I \underset{k_{-1}}{\overset{k_1}{\rightleftharpoons}} E\cdots I \underset{k_{-2}}{\overset{k_2}{\rightleftharpoons}} E - I$$

Figure 4. Reaction scheme for covalent inhibition. *E*, enzyme; *I*, inhibitor; *E*···*I*, noncovalent complex; k_1, association rate constant; k_{-1}, dissociation rate constant.

noncovalently (*E*···*I*) and then react to form a chemical bond (reversible in our present study) with their targets (*E*–*I*). Consequently, whereas the potency and selectivity of conventional noncovalent bond forming drugs are typically expressed in terms of equilibrium binding affinity, it is essential to consider the time-dependence of inhibition for covalent drugs (i.e., IC_{50}'s vary over time for reversible covalent inhibitors).[30]

Docking Covalent Inhibitors. We previously found that our current scoring function could distinguish between inactive and active inhibitors and can be used successfully in prospective studies.[15] However, it is not accurate enough to rank covalent inhibitors that are within 2 orders of magnitude in K_i. When optimizing our previous chemical series, we observed that the focus should be on the key interactions mentioned above. Selected docking data is summarized in Table 1 and Figure 5.

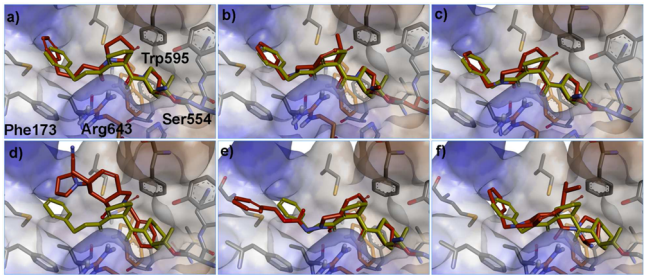

Figure 5. Structure-based design of potential covalent POP inhibitors. (a) Cocrystallized ligand (PDB code: 2xdw) together with known inhibitor **4** docked; (b) **8a**, R^1 = Me, R^2 = Bn; (c) **8a**, R^1 = H, R^2 = Bn; (d) **8b**, R^1 = Me, R^2 = Bn; (e) **8a**, R^1 = H, R^2 = CbzNH; (f) **8a**, R^1 = *i*-Pr, R^2 = Bn.

Both the scores computed using RankScore (a force field-based scoring function, the lower, the better) and MatchScore, which evaluates the match between the ligand and protein functional groups (the higher, the better), are given. MatchScore is instrumental in automatically measuring the key interactions, while RankScore evaluates other factors such as internal strain energy.

It is worth mentioning that a docking mode in which both noncovalent and covalent binding were investigated concomitantly was used. The results shown in Table 1 were collected for the lowest-in-energy poses, although in half of the cases, both covalent and noncovalent poses were proposed by FITTED. Care must be taken when analyzing the data as, in contrast to noncovalent binding, kinetic and thermodynamic factors control whether the binding will be covalent. If the lowest-energy pose is covalent, it suggests that the fit of the compound (first equilibrium in Figure 4) favorably positions the nitrile group leading to covalent inhibition. This mode of binding is optimal. If the lowest-energy pose is noncovalent but the second lowest-energy pose is covalent and with a score within 1–2 kcal/mol of the best pose, we still considered targeting the covalent molecule. In these cases, we anticipate that the affinities of the covalent and noncovalent inhibitors are comparable (uncertainties in our predicted binding energies are on the order of a few kcal/mol); however, we expect the

Table 1. Selected Docking Data

entry	R^1	R^2	scaffold	RankScore	MatchScore	binding
1	Me	Bn	**8a**	−15.9	107.9	covalent
2	Me	Bn	**8b**	−7.4	105.4	noncovalent
3	Me	Bn	*ent*-**8a**	−9.4	116.2	noncovalent
4	H	Bn	**8a**	−16.2	112.5	covalent
5	H	Bn	**8b**	−15.3	109.5	covalent
6	H	Bn	*ent*-**8a**	−11.2	106.6	noncovalent
7	Et	Bn	**8a**	−13.8	105.1	covalent
8	iPr	Bn	**8a**	−10.3	97.1	noncovalent
9	Ph	Bn	**8a**	−9.9	104.2	noncovalent
10	H	CbzNH	**8a**	−16.0	69.9	covalent
11	H	BnO	**8a**	−14.6	94.0	covalent
12	H	BnCONH	**8a**	−16.2	83.5	covalent
13			**9a**	−12.2	113.4	noncovalent
14			ent-**9a**	−10.2	64.0	covalent
15			**4**	−15.6	107.6	covalent

DOI: 10.1021/acs.jmedchem.5b01296
J. Med. Chem. XXXX, XXX, XXX–XXX

covalent molecule to have more favorable binding kinetics, i.e., longer bound lifetimes. The relatively high energy barrier to breaking the covalent bond leads in general to lower values of the dissociation constant, k_{off}. Thus, when noncovalent binding was suggested by the docking program, a close look at the other proposed poses was required. In addition, when docking potential covalent inhibitors, the reactivity of the warhead may differ. In the present study, only nitrile derivatives with expected similar reactivity were investigated.

First, the docking indicated that the diastereomeric scaffold **8a** with the absolute configuration shown in Figure 2 was preferred over the other diastereomers including **8b** and ent-**8a** to form a covalent bond with the enzyme (Table 1, entries 1−3 and 4−6). The same trend was consistently observed when docking was carried out with other R^1 and R^2 groups. According to our prediction, increasing the size of R^1 would result in weaker binding when R^1 exceeded one carbon and even in noncovalent binding with R^1 = iPr and Ph Table 1, entries 1, 4, and 7−9). The data collected for R^2 were more ambiguous. For example, while RankScore suggested that R^2 = BnCONH with R^1 = H should be optimal (entry 12), MatchScore indicated that R^2 = H should be favored (entry 4). As a reference, a highly active compound (**4**) was docked and scored (Table 1). Interestingly, our best scoring designed inhibitor was predicted to be as strong as this subnanomolar compound (entries 4 and 15, Figure 5a).

As the key interactions were featured by the cocrystallized compound shown in yellow in Figure 5a, this compound was overlaid with our docked compounds, thus revealing whether the key interactions and overall binding were retained. For example, while the compounds shown in Figure 5b, c, and e appeared to bind in a manner similar to that of the cocrystallized ligand, the two compounds shown in Figure 5d (built around scaffold **8b**) or Figure 5f (with a large R^1 group) were not predicted to retain all of the key interactions with POP. This predicted loss of interactions was more accurately measured by MatchScore than by RankScore.

CHEMISTRY

Synthetic Strategy. We have previously reported an expedient synthesis of **10a** and **10b**[26] (Figure 6) and more

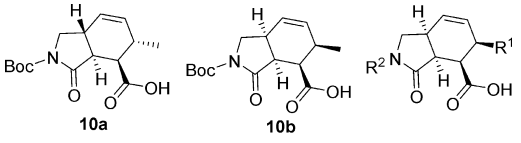

Figure 6. Generic structure of potential POP inhibitors.

recently optimized the synthetic protocol and investigated an observed solvent effect.[31] This new protocol enabled the selective precipitation of the major diastereomer, hence removing the need for extensive chromatography. We envisaged taking advantage of this synthetic strategy and probing its application to other analogues by varying R^1 and R^2.

Synthesis of Bicyclic Scaffolds Varying R^1 and R^2. According to the docking study, as long as R^1 is small enough, the potential inhibitor should fit in the POP binding site. These computational investigations were also indicating that R^2 of different sizes should fit, although with the shorter group preferred, and that the stereochemistry of the scaffold was critical. Accordingly, we restricted R^1 to only hydrogen and methyl, selected four groups of different lengths for R^2, and focused on scaffold **8a**, which is synthetically more accessible. The synthesis of these scaffolds required the conversion of two aldehydes into the corresponding hydrazides **12a−c**, alkoxyamine **12d**, and amines **12e** and **12f** (Table 2).

Table 2. Scaffold Synthesis

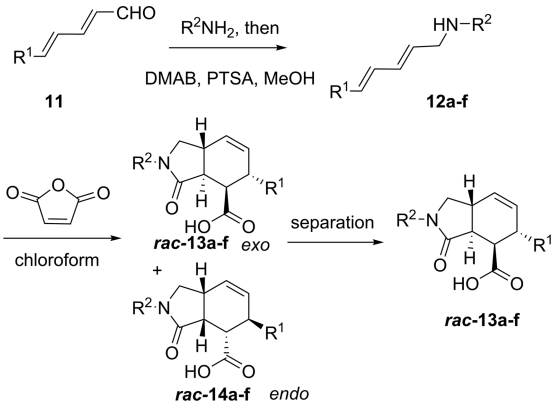

entry	R^1	R^2	Product 12[a,b]	Product 13[a,c]
1	H	NH-Cbz	**12a** (73%)	**13a** (65%)
2	Me	NH-Cbz	**12b** (94%)	**13b** (55%)
3	H		**12c** (55%)	**13c** (48%)
4	H	O-Bn	**12d** (31%)	**13d** (59%)
5	H	Bn	**12e** (31%)	**13e** (65%)
6	Me	Bn	**12f** (64%)	**13f** (51%)

[a]Yields are given in parentheses. [b]Isolated yield for the first step (**11** to **12a−f**). [c]Isolated yield of the major diastereomer from **12a−f** to **13a−f**.

The initial formation of the unsaturated hydrazides or amines was achieved by a solventless condensation (R^1 = Me) or in methanol (R^1 = H). The chemoselective reduction was next achieved with dimethylamino borane for products **12a−d** and with $NaBH_4$ for products **12e−f**, as reported previously.[26] The six intermediates were subsequently reacted with maleic anhydride leading to mixtures of *exo* **13a−f** and *exo* **13a−f** products, with the *exo* adducts being the major isomers.

During our optimization of the synthetic methodology,[31] we solved the difficult separation of the diastereomers through diastereoselective precipitation. We were very pleased that this stereoselective precipitation was also possible with the proposed substitutions at position R^2. Thus, treatment of the diastereomeric mixture with a mixture of ether and hexane (or dichloromethane) led to selective precipitation of the major *exo* adduct in most cases (Figure 7). The relative stereoselectivity of the scaffolds was determined by 1D NOE and 2D NOESY experiments on the scaffolds and some derivatives as reported previously (Figure 8).[26] We were also pleased to obtain crystals of **13d** (Figure 8). Consequently, the selective precipitation of the *exo* adduct was unambiguously confirmed by X-ray crystallographic analysis.

This optimized strategy not only provided a single isolated diastereomer but also eliminated the need for chromatographic purification of the polar bicyclic scaffolds. In the case of **13c**, the precipitation was more problematic and was difficult to reproduce. The mixture remaining in the mother liquor was not further investigated.

DOI: 10.1021/acs.jmedchem.5b01296
J. Med. Chem. XXXX, XXX, XXX−XXX

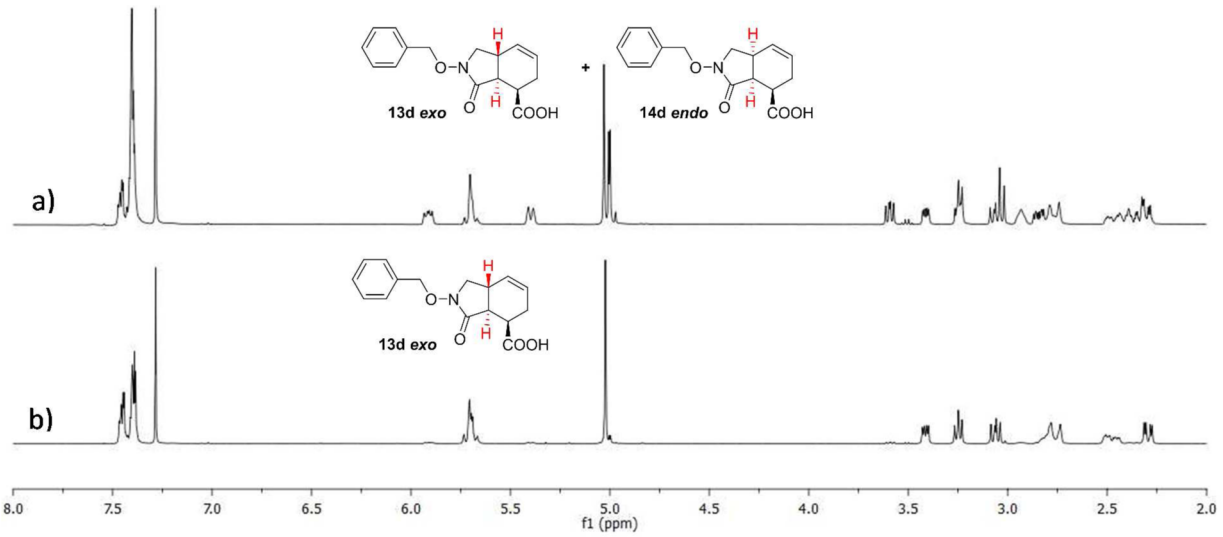

Figure 7. ^{1}H NMR spectrum of (a) a mixture of *endo* and *exo* adducts **14d** and **13d**; (b) *exo* adduct **13d**.

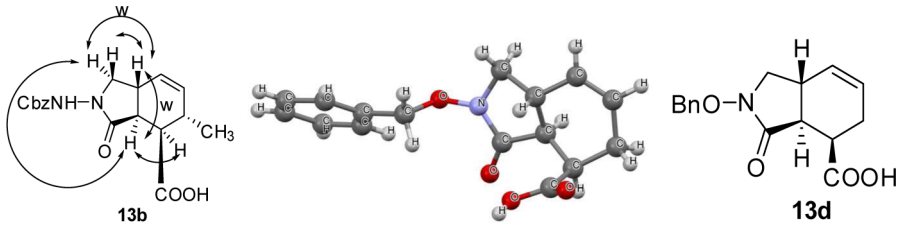

Figure 8. Stereochemistry of scaffolds **13b** ascertained by NOESY and the structure of **13d** determined by X-ray crystallography (oxygens in red, nitrogen in blue, carbons in gray, and hydrogens in light gray).

Synthesis of Potential Inhibitors. The synthesis of various derivatives of **7** is shown on Table 3. Following the strategy described above, the scaffolds **13a–f** with the *exo* configuration were diastereopure yet racemic.[26] Compound **13a** was next converted into the corresponding nitrile derivative **9a** by an amidation/dehydration sequence in reasonable yields. As the modeling study suggested that this series should not lead to significant activity, no other derivatives were prepared. The potential covalent inhibitors **7a–f** and **16a–f** were accessed by coupling with (*S*)-cyano-pyrrolidine, while their noncovalent counterparts **15a–f** were prepared as racemic mixtures through coupling with pyrrolidine. Although the scaffold **8a** was our priority, *ent*-**8a** analogues were produced along with **8a** analogues. The other scaffolds (R^1 = other than H and methyl) were not synthesized since the docking study predicted that increased steric bulk at that position would either affect the potency (RankScore) or disrupt the covalent binding.

Extensive chromatographic work enabled the separation of the diastereomers resulting from coupling the racemic scaffolds (including *rac*-**13d**) to enantiopure (*S*)-cyano-pyrrolidine. While the relative stereochemistry of *rac*-**13d** and other scaffolds was assigned by X-ray crystallography and NMR spectroscopy, determination of the stereochemistry of the resulting pairs of diastereomers (such as enantiopure **7d** and **16d** from *rac*-**13d**) was difficult until we managed to crystallize **16d** (Figure 9). While crystallography assigned the relative stereochemistry, the absolute stereochemistry was derived knowing the absolute stereochemistry of (*S*)-cyano-pyrrolidine, which was coupled in this process. Interestingly, the NMR spectra of **7d** and **16d** were significantly different revealing a mixture of rotamers for **16d** only. Similarly, **7c** and **7e** appeared as a single averaged conformation on NMR spectra, while the NMR signatures of **16c** and **16e** were more complex (Figure 9). Using the crystal structure as a starting point and the NMR similarities, we were able to ascertain the relative and absolute stereochemistries of these 12 compounds. This solved a structural assignment challenge that was foreseen to be difficult.

BIOLOGICAL EVALUATIONS

Inhibition of POP. As discussed above, the binding is a two-step process, including a fast binding and a slow covalent bond formation. Thus, the inhibition potencies were measured after equilibria were reached. With this in mind, the 19 synthesized compounds were assessed for their inhibitory potency on recombinant human POP (Tables 4 and 5) and their activities compared to our computational predictions (Table 6). Gratifyingly, an excellent match between experimental data and computational predictions was observed. In order to summarize the information gained, we will examine the most notable results of this study.

First, we noted that rigidifying the right side of the cocrystallized structure (i.e., compound **9a**) did not lead to any noticeable activity and was, as predicted, detrimental to binding. Second, the potentially covalent inhibitors (featuring a nitrile group) were found to be more potent than their noncovalent counterparts. For example, **15d** is 3 orders of magnitude less active than **7d**. This difference is much more pronounced than that in our previous chemical series for which an order of magnitude was the norm. Third, the absolute stereochemistry of the scaffold was a key factor, as demonstrated with **16c**, **16d**, **16e**, and **16f** being micromolar at best, while **7c**, **7d**, **7e**, and **7f** were nanomolar inhibitors with

DOI: 10.1021/acs.jmedchem.5b01296
J. Med. Chem. XXXX, XXX, XXX–XXX

Table 3. Potential POP Inhibitor Synthesis

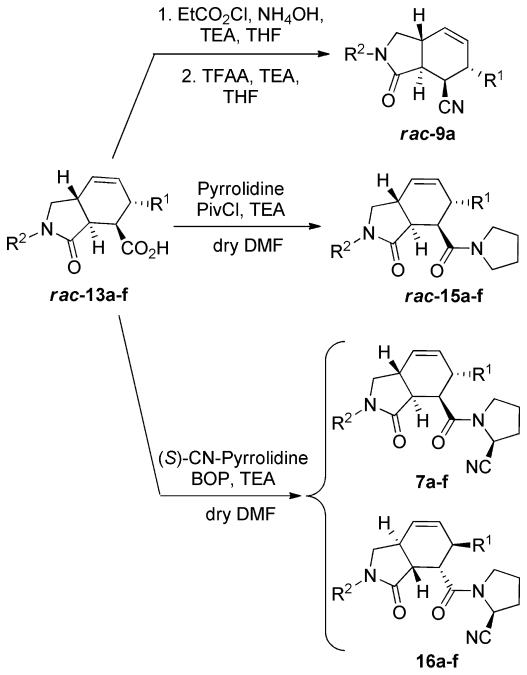

entry	compd	R^1	R^2	Product (yield, %)
1	**13a**	H	NH-Cbz	**9a** (75)
2	**13a**	H	NH-Cbz	**15a** (16)
3	**13b**	Me	NH-Cbz	**15b** (61)
4	**13c**	H		**15c** (30)
5	**13d**	H	O-Bn	**15d** (51)
6	**13e**	H	Bn	**15e** (58)
7	**13f**	Me	Bn	**15f** (71)
8	**13a**	H	NH-Cbz	**7a**/**16a** (34)
9	**13b**	Me	NH-Cbz	**7b**/**16b** (64)
10	**13c**	H		**7c**/**16c** (15)
11	**13d**	H	O-Bn	**7d**/**16d** (66)
12	**13e**	H	Bn	**7e**/**16e** (31)
13	**13f**	Me	Bn	**7f**/**16f** (73)

7e being the most active (K_i = 1 nM). There are cases (i.e, fluoxetine, an antidepressant)[32] in which the changes in stereochemistry do not substantially affect the potency. In the case of noncovalent drugs, their position and orientation within the binding site can adjust to optimize interactions. However, the formation of a covalent bond provides less opportunity for the drug to adjust its binding. As a result, the stereochemistry difference between **7e** and **16e**, although four bonds away from the "covalent group", was not tolerated. Fourth, the introduction of an R^1 group even as small as methyl was detrimental to the activity (**15e** vs **15f**, Table 4). This observation was in line with the predictions. Fifth, the size of the R^2 group can be used to modulate the affinity. Our docking study showed that a benzyl group (**7e**: K_i = 1.0 nM) would be the optimal size, while longer chains would be tolerated, with the best fit for benzyl and the worst with Cbz. The increasing size of this appendage correlated with a predicted increase in distance from the side chain of Phe173.

Our survey of the field revealed that the hydrophobic interaction is not as critical for the binding as are the two

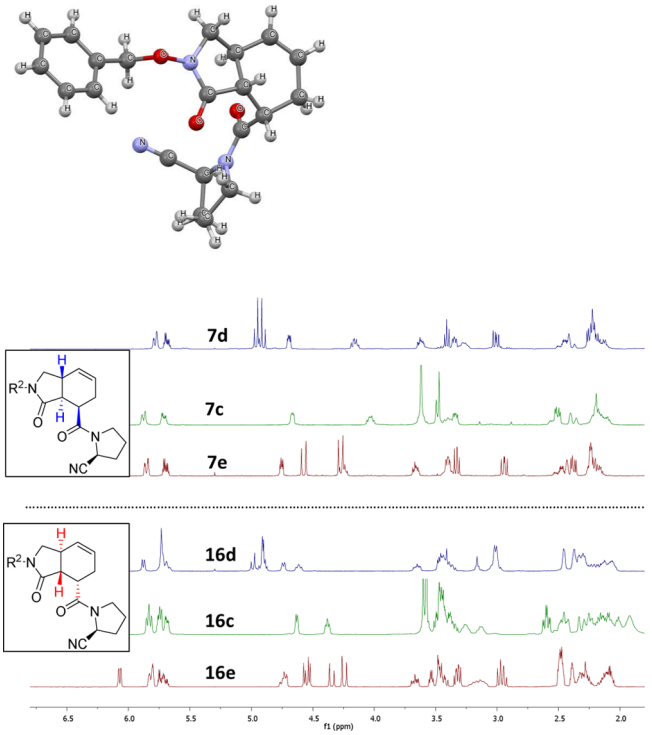

Figure 9. Structure of **16d** (oxygens in red, nitrogens in blue, carbons in gray, and hydrogens in light gray) as determined by X-ray crystallography and ^{1}H NMR spectra of the enantiopure compounds.

Table 4. Inhibition of POP

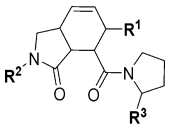

compd	R^1	R^2	R^3	POP, K_i (μM)
6	-	-	CN	0.023
9a	H	NH-Cbz	H	>150
15a	H	NH-Cbz	H	12 ± 1
15b	Me	NH-Cbz	H	67 ± 5
15c	H		H	65 ± 12.5
15d	H	O-Bn	H	7.5 ± 1.5
15e	H	Bn	H	0.0325 ± 0.0025
15f	Me	Bn	H	1 ± 0.05
7a	H	NH-Cbz	CN	1.5 ± 0.1
16a	H	NH-Cbz	CN	80 ± 5
7b	Me	NH-Cbz	CN	62.5 ± 10
16b	Me	NH-Cbz	CN	>150
7c	H		CN	4 ± 0.45
16c	H		CN	>150
7d	H	O-Bn	CN	0.01 ± 0.001
16d	H	O-Bn	CN	>150
7e	H	Bn	CN	0.001 ± 0.00005
16e	H	Bn	CN	2.1 ± 0.15
7f	Me	Bn	CN	0.046 ± 0.0025
16f	Me	Bn	CN	62 ± 15

DOI: 10.1021/acs.jmedchem.5b01296
J. Med. Chem. XXXX, XXX, XXX−XXX

Table 5. Tight Binding Inhibition with 4 and 7e

inhibitor	Morrison K_i (tight binder) (nM)	regular K_i (nM)
4	0.92 ± 0.02	0.95 ± 0.15
7e	0.75 ± 0.02	1.33 ± 0.15

Table 6. Docking-Based Predictions vs Experiments

prediction	example	experiment
scaffold on the left side > scaffold on the right side	**9** vs **7**	correct
covalent more active than noncovalent	**7** vs **15**	correct
stereochemistry: 3S,4R,7R > 3R,4S,7S	**7e** vs **16e**	correct
R^1 = H, Me equally tolerated	**15e**, **15f**	Me tolerated but less than H
R^2 = Bn > OBn > $C(O)CH_2Ph$ > NHCbz	**16a**, **16c**, **16d**, **16e**	correct
4 and **7e** should be equally potent	**4** vs **7e**	correct

above-mentioned hydrogen bonds and the covalent bond.[1] In agreement with these previous observations, disrupting this hydrophobic interaction led to decreased potency, although less pronounced than breaking the covalent bond or the hydrogen bonds.

In a previous report, Venäläinen et al. reported a K_i of 0.023 nM for inhibitor **4**,[8] nearly 2 orders of magnitude more potent than **7e** (K_i = 1.0 nM), while our docking studies indicated similar activities for these two compounds. In order to compare the two inhibitors under the same conditions, we carried out a second set of experiments with **7e** and **4** following the procedure of Venäläinen et al., who computed the K_i using the Morrison equation which considers tight binding.[33] In our experiments (Table 5), we observed that **4** and **7e** were nearly as potent.

Overall, this study identified a highly potent POP inhibitor (**7e**, K_i = 1.0 nM), exhibiting potency on par with the most active compounds reported to date (Figure 1) including those moved to clinical trials.[1]

Metabolism Studies. One of the concerns that was raised while this work was ongoing was the numerous possible sites of metabolism on this class of scaffolds. In fact, our first chemical series illustrated by **5** was terminated due to the high complexity of its metabolism, leading to several potentially toxic metabolites.[34] The epoxidation of aromatic rings and double bonds by cytochrome P450 enzymes present in the liver is one of the major causes of drug withdrawal and therefore should be carefully examined early in the drug discovery and development process.[35−37] In our lead compound **7e**, both the double bonds and the *N*-benzyl moiety may lead to reactive metabolites and/or low metabolic stability (reduced half-life). In fact, the former may be prone to epoxidation leading, while the latter may undergo *N*-dealkylation. Unexpectedly, **7e** was found to be very stable in human liver microsomes (Cl_{int} = 4 μL/min/mg protein) and even more stable than our previous lead **6**. Under the experimental conditions used, no N-debenzylated products were observed, and only trace amounts of mono-oxidation metabolites were detected.

CONCLUSIONS

The first use of 3-oxo-hexahydro-1*H*-isoindole-4-carboxylic acid as a chiral drug template is presented. Structure-based guided design and efficient synthesis led to the discovery of a highly potent POP inhibitor (**7e**) exhibiting single digit nanomolar activity (K_i = 1.0 nM), significantly lower than that of our previous hit (**6**, K_i = 23.0 nM) and similar to the potencies of POP inhibitors which have entered clinical trials such as KYP-2047.[1] In addition, this novel lead molecule **7e** showed improved metabolic stability over our previous leads. Thus, **7e** will now be moved to *in vivo* studies.

Interestingly, this chemical series was also used to assess our computational predictions and confirmed that the current version of FITTED can be used to guide the design of active covalent inhibitors.

This successful study together with our previous reports improves our understanding of the geometrical requirements for optimal POP inhibition as well as our comprehension of covalent inhibition, in both computational and experimental perspectives.

EXPERIMENTAL SECTION

Protein Expression. *E. coli* BL21 competent cells were transformed with pETM10 hPOP. A starter culture of LB medium (100 mL) containing kanamycin (50 mg mL^{-1}) was inoculated with one colony and was incubated overnight at 37 °C with shaking. After 16 h, four cultures of LB (4 × 1000 mL) containing kanamycin (50 mg mL^{-1}) were inoculated with the overnight culture (20 mL). The inoculated cultures were incubated at 37 °C and 220 rpm until the OD600 was between 0.3 and 0.5 (3 h). The temperature was lowered to 18 °C, IPTG was added (final concentration of 0.5 mM), and induction was allowed to proceed for 5 h. Cells were harvested by centrifugation (4000*g*, 15 min, 4 °C), and the pellet was resuspended in suspension buffer (50 mL) [Tris-HCl (10 mM), NaCl (300 mM), β-mercaptoethanol (5 mM), imidazole (1 mM), and 5% glycerol, pH 8] and sonicated for four cycles (2 min of sonication/2 min of rest; pulse, 0.5 intensity; duty, 0.5), while the sample was kept on ice (Branson sonifier 450, Emerson industrial automation, United States). After sonication, the sample was centrifuged (40000*g*, 30 min, 4 °C), and the supernatant was used immediately for POP purification. An affinity column was used (10 mL, Toyopearl, AF-Chelate-650M) for purification. The supernatant was applied at a flow rate of 0.5 mL min^{-1} to a column previously equilibrated with 5 column volumes of $NiSO_4$ (0.2 M) followed by 5 column volumes of suspension buffer. The column was then washed with suspension buffer until the absorbance at 280 nm returned to basal level. The column was then rinsed with 5 column volumes of washing buffer [Tris-HCl (20 mM), NaCl (300 mM), β-mercaptoethanol (5 mM), imidazole (15 mM), and 5% glycerol, pH 8]. The elution was then performed with 4 column volumes of elution buffer [Tris-HCl (20 mM), NaCl (300 mM), β-mercaptoethanol (5 mM), imidazole (500 mM), and 5% glycerol, pH 8]. Fractions (4 mL) were collected during the entire elution. Fractions testing positive for POP activity (REF) were analyzed by SDS−PAGE and stained with phastgel blue R (GE Healthcare, sweden). POP-containing fractions were combined and subjected to size exclusion chromatography (HiLoad 16/60 Superdex75 prep grade on a Amersham Biosciences FPLC system) with [Tris-HCl (20 mM), NaCl (150 mM), benzamidine (5 mM), EDTA (1 mM), β-mercaptoethanol [5 mM], and 5% glycerol, pH 8] as the running buffer. The purified enzyme was dialyzed into the appropriate buffer. Recombinant hPOP was quantified by measuring the absorbance at 280 nm using an extinction coefficient calculated by the following equation (ε = nTrp*5000 + nTyr*1490 + nCys*125, 129090 $L{\cdot}mol^{-1}{\cdot}cm^{-1}$ for POP[38]). Aliquots of the recombinant enzyme were prepared and immediately frozen with liquid nitrogen and stored at −80 °C.

POP Activity Assays. *Chemicals and Reagents.* ZGP-pNA was obtained from Bachem (Bubendorf, Switzerland).

IC_{50}/K_i Measurement. The reactions were performed in microtiter plates of 96 wells. For each reaction, the activity buffer (A.B.) (140 μL, sodium phosphate (20 mM), NaCl (150 mM), β-mercaptoethanol (5 mM), EDTA (2 mM), 10% glycerol, and 0.5 mg/mL BSA, pH 8) was preincubated for 30 min at 30 °C with hPOP (20 μL, 10 nM in A.B.)

DOI: 10.1021/acs.jmedchem.5b01296
J. Med. Chem. XXXX, XXX, XXX−XXX

and with the corresponding inhibitor solution (20 μL) or activity buffer (controls). Stock inhibitors were prepared in DMSO (100 mM); dilutions for inhibitor evaluation were prepared from the stock in the activity buffer. A control experiment with the same DMSO concentration was performed. After preincubation, ZGP-pNA (20 μL, 0.8 mM in A.B., final concentration of 80 μM) was added, and the formation of the product was followed by absorbance at 405 nm every 30 s. Initial velocity was measured for each concentration of inhibitor and compared to the initial velocity of reactions that did not contain inhibitor. The IC_{50} value was defined as the inhibitor concentration causing a 50% decrease in activity. The K_i was defined as $IC_{50}/(1+([S]/K_m))$. The K_m of the substrate has been measured by monitoring the initial velocity of the enzymatic reaction of 1 nM of hPOP with various concentrations of substrate. Data obtained were K_m = 74.6 μM; k_{cat} = 20.56 s^{-1}.

Morrison K_i. For **7e**, since the K_i was in the same range as the enzyme concentration used in the assay, the Morrison equation was used.[39] The same protocol as the IC_{50} was used with the appropriate concentration range. Initial velocities were determined in the presence (v_i) and the absence (v_0) of the inhibitor, and the subsequent ratio (v_i/v_o) was plotted against the inhibitor concentration and fitted to the Morrison equation:

$$\frac{v_i}{v_0} = 1 - \frac{(E + I + K_i^{app}) - \sqrt{(E + I + K_i^{app})^2 - 4EI}}{2E}$$

where E is the active enzyme concentration in the assay (1 nM here), I is the inhibitor concentration, and K_i^{app} is the apparent dissociation constant of the inhibitor. Similarly to that for the IC_{50}, knowing the Henri−Michaelis−Menten constant (K_m = 74.6 μM) and the substrate concentration used in the assay ([S] = 80 μM), it is possible to compute the true dissociation constant following this equation:

$$K_i = \frac{K_i^{app}}{\left(1 + \frac{[S]}{K_m}\right)}$$

Metabolism. Analyses were performed on an Agilent 1100 modular system equipped with an autosampler, a quaternary pump system, a photodiode array UV detector, a quadrupole MS detector, and a ChemStation (for LC 3D A.09.03) data system. Separation was achieved using a Zorbax Eclipse XDB-C18 150 mm × 4.6 mm, 5 μm. Elution consisted of a gradient step from 99% mobile phase A (H_2O) and 1% mobile phase B (CH_3CN), to 99% phase B over 20 min, at a flow rate of 1 mL/min. The absorption was recorded at 220 nm.

Docking. For the docking study, we used our docking program FITTED[40] (FORECASTER platform[41]), which was previously modified to account for covalent inhibitors.[15] The compounds were prepared for docking using our program SMART and docked to a protein structure prepared from the PDB file using PREPARE (PDB code: 2XDW) and further processed for use in docking studies using PROCESS. The docking was carried out with Ser554 identified as a catalytic residue susceptible to forming a covalent bond with reactive groups. FITTED uses a genetic algorithm as a conformational search algorithm. A maximum number of generation of 200 and a convergence criterion Diff_N_Best 0.25 (converged when the 20 lowest-in-energy individuals were within 0.25 kcal/mol) were used. These parameters ensured a more exhaustive conformation search. Default values were used for all the other parameters.

Crystallography. Crystal and molecular structures of **13d** and **16d** were determined by single crystal X-ray diffraction. Diffraction measurements were made on a Bruker D8 APEX2 X-ray diffractometer instrument using graphite-monochromated MoK_α (λ = 0.71073 Å) radiation. The X-ray diffraction data sets were collected using the ω scan mode over the 2θ range up to 54° at 100 K. The structures were solved by direct methods implemented in SHELXS and refined using SHELXL.[42] Structure refinement was performed on F^2 using all data, and hydrogen atoms were modeled with appropriate riding-hydrogen models on the carbon centers. Calculations were performed, and the drawings were prepared using the WINGX[43] suite of crystallographic programs. Compound **13d** crystallizes in a centrosymmetric space group $P2_1/n$ and is not enantiopure. Compound **16d** crystallizes in an enantiomorphic space group $P2_12_12_1$. There was insufficient anomalous scattering from the crystal due to the crystal diffracting poorly overall, even at a 100 K. Attempts to isolate a more suitable one were either unsuccessful or resulted in a crystal of approximately the same quality. The absolute structure of compound **16d** was determined in reference to a known chiral center which does not change in the synthetic procedure. Structures have been deposited with the Cambridge Structural Database, deposition codes CCDC 1430175-1430176.

Synthesis. All commercially available reagents were used without further purification unless otherwise stated. The 4 Å molecular sieves were dried at 100 °C prior to use. Optical rotations were measured on a JASCO DIP 140 in a 1 dm cell at 20 °C. FTIR spectra were recorded using a PerkinElmer Spectrum One FT-IR. ^1H and ^{13}C NMR spectra were recorded on Varian Mercury 400 MHz, 300 MHz, or Unity 500 spectrometers. Chemical shifts are reported in ppm using the residual of deuterated solvents as internal standard. Thin layer chromatography visualization was performed by UV or by development using $KMnO_4$, H_2SO_4/MeOH, or Mo/Ce solutions. Chromatography was performed on silica gel 60 (230−40 mesh). Low resolution mass spectrometry was performed by ESI using a Thermoquest Finnigan LCQ Duo. High resolution mass spectrometry was performed by EI peak matching (70 eV) on a Kratos MS25 RFA double focusing mass spectrometer or by ESI on a Ion Spec 7.0 T FTMS at McGill University. Prior to biological testing, reversed phase HPLC was used to verify the purity of compounds on an Agilent 1100 series instrument equipped with a VWD-detector, a C18 reverse column (Agilent, Zorbax Eclipse XDB-C18 150 mm 4.6 mm, 5 μm), and UV detection at 254 or 220 nm. All tested compounds were at least 95% pure. All measured purities are listed in Table 7.

Table 7. HPLC Analysis of Purity

compd	retention time (min)[a]	purity (%)
9a[b]	16.4	90.4
15a[b]	18.0	97.6
15b	18.8	96.7
15c[b]	16.7	98.1
15d	17.5	96.0
15e	18.6	96.5
15f	19.5	95.5
7a[b]	17.3	96.5
16a[b]	17.1	99.0
7b[b]	18.1	96.1
16b[b]	18.1	98.6
7c[b]	16.0	99.9
16c[b]	15.7	98.7
7d[b]	17.1	92.0
16d	17.2	97.2
7e[b]	17.6	98.5
16e	17.6	95.6
7f[b]	18.7	98.2
16f[b]	18.7	95.0

[a]Conditions: (95% water, 5% methanol, and 1 mL/min). [b]UV detection at 220 nm.

General Procedure for the Reductive Amination of Aldehydes. To a solution of Cbz-hydrazide or amine (1 equiv) in MeOH (concentration of 1 M) was added a solution of dienal (1 equiv) in DCM dropwise. The mixture was stirred for 30 min at room temperature. The solution was cooled to 0 °C, and $Me_2NH{\cdot}BH_3$ (1.5 equiv) was added slowly, followed by a solution of pTSA (6 equiv) in MeOH (concentration 1 M). After stirring for another 2 h, a solution of Na_2CO_3(aq) (2-fold dilution, 10% w/v) was added, and the mixture was stirred for 2 h then concentrated under reduced pressure, extracted with CH_2Cl_2, washed with brine, dried over Na_2SO_4, and

DOI: 10.1021/acs.jmedchem.5b01296
J. Med. Chem. XXXX, XXX, XXX−XXX

concentrated under reduced pressure. The crude product was purified by flash chromatography with eluent Hex/EtOAc to afford the desired product.

Benzyl 2-((2*E*)-penta-2,4-dienyl)hydrazinecarboxylate (12a). Yield: 73%. IR (film) ν_{max} (cm^{-1}) 3314.85, 2972.36, 2891.14, 1686.76; ^1H NMR (300 MHz, $CDCl_3$) δ (ppm) 7.45−7.30 (m, 5H), 6.32 (dt, J = 16.7, 10.2 Hz, 1H), 6.25−6.15 (m, 1H), 5.76−5.62 (m, 1H), 5.20 (d, J = 16.5 Hz, 1H), 5.14 (s, 2H), 5.11−5.02 (m, 1H), 3.58−3.48 (m, 2H); ^{13}C NMR (75 MHz, $CDCl_3$) δ (ppm) 157.2, 136.3, 136.0, 134.5, 129.2, 128.6 128.3, 128.2, 117.5, 67.1, 53.5; HRMS (ESI+) for $C_{13}H_{17}N_2O_2$ (M + H) calcd, 233.12900; found, 233.12770.

Benzyl 2-((2*E*,4*E*)-hexa-2,4-dienyl)hydrazinecarboxylate (12b). Yield: 94%. IR (film) ν_{max} (cm^{-1}) 3274.60, 3019.77, 2912.85, 1702.27; ^1H NMR (300 MHz, $CDCl_3$) δ (ppm) 7.31 (s, 5H), 6.72 (bs, 1H), 6.06 (m, 2H), 5.64 (dq, J = 6.7, 13.5 Hz, 1H), 5.51 (dd, J = 7.1, 14.6 Hz, 1H), 5.10 (s, 2H), 4.25 (bs, 1H), 3.45 (d, J = 5.4 Hz, 2H), 1.72 (d, J = 6.6 Hz, 3H); ^{13}C NMR (75 MHz, $CDCl_3$) δ (ppm) 157.2, 136.2, 134.3, 130.9, 129.8, 128.6, 128.2, 128.2, 125.8, 67.0, 25.3, 18.1; HRMS (ESI+) for $C_{14}H_{18}N_2O_2Na$ (M + Na) calcd, 269.1266; found, 269.1265.

(*E*)-*N*′-(Penta-2,4-dien-1-yl)-2-phenylacetohydrazide (12c). White solid. R_f = 0.15 (Hex/EtOAc, 5:5). Yield: 55%. IR (film) ν_{max} (cm^{-1}) 3275, 3083, 2924, 1645, 1454, 1348, 1005; ^1H NMR (400 MHz, $CDCl_3$) δ (ppm) 7.45−7.07 (m, 5H), 6.26 (dt, J = 16.8, 10.2 Hz, 1H), 6.08 (dd, J = 15.2, 10.5 Hz, 1H), 5.66−5.50 (m, 1H), 5.14 (d, J = 16.6 Hz, 1H), 5.05 (d, J = 10.1 Hz, 1H), 4.29 (bs, 1H), 3.49 (s, 2H), 3.38 (bd, J = 5.6 Hz, 2H); ^{13}C NMR (75 MHz, $CDCl_3$) δ (ppm) 170.5, 136.3, 134.8, 134.2, 129.4 (2C), 129.2, 129.0 (2C), 127.5, 117.6, 53.6, 42.1; HRMS (ESI +) for $C_{13}H_{17}N_2O$ (M + H) calcd, 217.1335; found, 217.1337.

(*E*)-*O*-Benzyl-*N*-(penta-2,4-dien-1-yl)hydroxylamine (12d). Colorless oil. Yield: 31%. R_f = 0.36 (Hex/EtOAc, 9:1); IR (film) υ_{max} (cm^{-1}) 3265, 3087, 1603; ^1H NMR (500 MHz, $CDCl_3$) δ (ppm) 7.37−7.28 (m, 5H), 6.34 (dt, J = 15.0, 10.0 Hz, 1H), 6.25−6.20 (m, 1H), 5.77 (dt, J = 15.0 Hz, 5.0 Hz, 1H), 5.19 (d, J = 15.0 Hz, 1H), 5.08 (d, J = 10 Hz, 1H), 4.72 (s, 2H), 3.58 (d, J = 5.0 Hz, 2H); ^{13}C NMR (125 MHz, $CDCl_3$) δ (ppm) 137.9, 136.6, 134.2, 129.6, 128.6, 128.5, 128.0, 117.3, 76.4, 54.1; HRMS (ESI+) for $C_{12}H_{16}NO$ (M + H) calcd, 190.1226; found, 190.1201.

(*E*)-*N*-Benzylpenta-2,4-dien-1-amine (12e). A solution of dienal (800 mg, 9.74 mmol) and benzylamine (1.04 g, 9.74 mmol) was stirred 2 h at room temperature. Then, the reaction mixture was cooled to 0 °C and allowed to stir for an additional 30 min. To the mixture was added $NaBH_4$ (1.47 g, 38.96 mmol), and the resulting mixture was allowed to stir for 2 h. The reaction mixture was quenched with H_2O and extracted with DCM. The combined organic layer was washed with 10% NaOH, brine, dried over Na_2SO_4, filtered, and evaporated. The crude product was chromatographed on silica gel with eluent Hex/EtOAc 9:1, to give a colorless oil. Yield: 500 mg (31%). R_f = 0.23 (Hex/EtOAc 7:3). Spectral data were consistent with data reported in the literature.[44]

(2*E*,4*E*)-*N*-Benzylhexa-2,4-dien-1-amine (12f). After stirring a solution of hexadienal (2.07 g, 21.6 mmol) and benzylamine (2.35 mL, 21.6 mmol) in MeOH (18 mL) for 2 h at room temperature, the mixture was cooled to 0 °C and allowed to stir for an additional 30 min. To the mixture was added $NaBH_4$ (1,6 g, 43.2 mmol), and the resulting mixture was allowed to stir for an additional hour. The reaction mixture was quenched with H_2O and extracted with DCM. The combined organic layer was washed with NaOH 10%, brine, dried over Na_2SO_4, filtered, and evaporated. The crude product was chromatographed on silica gel gel with eluent Hex/EtOAc 9:1, to give a yellow oil. Yield: 2,6 g (64%). R_f = 0.35 (Hex/EtOAc 5:5). Spectral data were consistent with data reported in the literature.[44]

General Procedure for Lactam Formation/Diels−Alder Reaction. To a solution of diene (1 equiv) in $CHCl_3$ (to a concentration of 0.25M) was added maleic anhydride (1 equiv). After stirring for 15 h, the solution was concentrated under reduced pressure, and the two diastereomers were separable by precipitation in a mixture of ether/DCM or by flash chromatography (Hex/EtOAc) to afford the *exo* product.

***rac*-(3a*S*,4*S*,7a*S*)-2-(((benzyloxy)carbonyl)amino)-3-oxo-2,3,3a,4,5,7a-hexahydro-1*H*-isoindole-4-carboxylic Acid (13a).** White solid. Yield: 99% (for all isomers) *exo* adduct: 65%. IR (film) ν_{max} (cm^{-1}) 3030, 2941, 2922, 2853, 1739, 1720, 1709; ^1H NMR (400 MHz, $CDCl_3$) δ (ppm) 7.40−7.20 (m, 5H), 5.77 (bd, J = 10.0 Hz, 1H), 5.67 (bd, J = 6.9 Hz, 1H), 5.14 (s, 2H), 3.58 (dd, J = 7.5, 7.4 Hz, 1H), 3.50−3.41 (m, 1H), 3.40−3.31 (m, 1H), 3.10−3.00 (m, 1H), 2.68 (bd, J = 20.0 Hz, 1H), 2.45−2.40 (m, 1H); ^{13}C NMR (125 MHz, $CDCl_3$) δ (ppm) 175.4 (2C), 155.3, 135.5, 128.6, 128.5 (2C), 128.3 (2C), 127.8, 125.1, 67.8, 45.1, 40.3, 35.8, 32.7, 28.1; HRMS (ESI-) for $C_{17}H_{17}N_2O_5$ (M − H) calcd, 329.11430; found, 329.11429.

***rac*-(3a*S*,4*R*,5*S*,7a*R*)-2-(((Benzyloxy)carbonyl)amino)-5-methyl-3-oxo-2,3,3a,4,5,7a-hexahydro-1*H*-isoindole-4-carboxylic Acid (13b).** White solid. Yield: 55%. IR (film) ν_{max} (cm^{-1}) 3251, 3024, 2960, 1706; ^1H NMR (400 MHz, $CDCl_3$) δ (ppm) 7.38−7.30 (m, 5H), 7.23 (brs, NH), 5.76 (d, J = 9.6 Hz, 1H), 5.60 (d, J = 9.6 Hz, 1H), 5.19−5.12 (m, 2H), 3.56 (t, J = 7.2 Hz, 1H), 3.46−3.33 (m, 2H), 2.99−2.92 (m, 3H), 2.42 (d, J = 7.2 Hz, 1H), 1.15 (d, J = 7.2 Hz, 3H); ^{13}C NMR (125 MHz, $CDCl_3$) δ (ppm) 175.8, 174.6, 155.5, 135.7, 134.1, 128.9, 128.7, 128.5, 124.4, 67.9, 42.9, 42.5, 33.3, 32.9, 21.8; HRMS (ESI+) for $C_{18}H_{20}N_2O_5Na$ (M + Na) calcd, 367.1269; found, 367.1275.

***rac*-(3a*S*,4*R*,7a*R*)-3-oxo-2-(2-Phenylacetamido)-2,3,3a,4,5,7a-hexahydro-1*H*-isoindole-4-carboxylic Acid (13c) and *rac*-(3a*S*,4*R*,7a*S*)-3-oxo-2-(2-Phenylacetamido)-2,3,3a,4,5,7a-hexahydro-1*H*-isoindole-4-carboxylic Acid (14c).** White solid. Yield: 48%. R_f = 0.24 (DCM/MeOH, 97:3). IR (film) ν_{max} (cm^{-1}) 3214, 3027, 2924, 1716, 1670, 1661, 1195; ^1H NMR (500 MHz, $CDCl_3$) δ 8.31 (s, 0.5H), 7.84 (s, 0.5H), 7.41−7.27 (m, 5H), 5.98−5.83 (m, 0.5H), 5.78 (d, J = 10.0 Hz, 0.5H), 5.68 (dd, J = 10.0, 3.4 Hz, 0.5H), 5.57 (d, J = 9.4 Hz, 0.5H), 3.94 (dd, J = 15.2, 8.3 Hz, 0.5H), 3.61 (dd, J = 10.6, 6.7 Hz, 2H), 3.56−3.44 (m, 1.5H), 3.41 (dd, J = 7.5, 3.4 Hz, 0.5H), 3.33 (dd, J = 7.9, 3.4 Hz, 0.5H), 3.20 (d, J = 9.1 Hz, 0.5H), 3.07 (bs, 0.5H), 2.94 (bs, 0.5H), 2.87−2.76 (m, 0.5H), 2.70 (d, J = 18.8 Hz, 0.5H), 2.56−2.39 (m, 1H), 2.38−2.22 (m, 0.5H). ^{13}C NMR (125 MHz, $CDCl_3$) δ 176.0, 175.9, 174.0, 170.5, 170.1, 167.5, 133.9, 133.5, 129.5, 129.47, 129.2, 129.0, 128.7, 128.0, 127.7, 127.5, 126.9, 125.2, 53.8, 52.4, 45.1, 41.4, 41.3, 40.5, 39.2, 36.0, 33.1, 32.7, 28.2, 23.7; HRMS (ESI−) for $C_{17}H_{17}N_2O_4$ (M − H) calcd, 313.1194; found, 313.1193.

***rac*-(3a*R*,4*S*,7a*S*)-2-(Benzyloxy)-3-oxo-2,3,3a,4,5,7a-hexahydro-1*H*-isoindole-4-carboxylic Acid (13d).** White solid. Yield: 59%. R_f = 0.24 (Hex/EtOAc 7:3). IR (film) ν_{max} (cm^{-1}) 3030, 1734, 1709; ^1H NMR (400 MHz, $CDCl_3$) δ (ppm) 7.44−7.42 (m, 2H), 7.39−7.36 (m, 3H), 5.71−5.64 (m, 2H), 5.00 (s, 2H), 3.39 (dd, J = 8.0, 3.6 Hz, 1H), 3.22 (t, J = 7.2 Hz, 1H), 3.04 (dd, J = 10.8, 7.6 Hz, 1H), 2.82−2.71 (m, 2H), 2.49−2.41 (m, 1H), 2.27 (dd, J = 12.4, 3.6 Hz, 1H); ^{13}C NMR (125 MHz, $CDCl_3$) δ (ppm) 176.0, 170.4, 135.3, 129.9 (2C), 129.1, 128.7 (2C), 127.9, 125.0, 77.5, 51.4, 44.9, 35.9, 31.9, 28.0; HRMS (ESI+) for $C_{16}H_{17}NO_4Na$ (M + Na) calcd, 310.1055; found, 310.1049.

***rac*-(3a*R*,4*S*,7a*S*)-2-Benzyl-3-oxo-2,3,3a,4,5,7a-hexahydro-1*H*-isoindole-4-carboxylic Acid (13e).** White solid. Yield: 65%. R_f= 0.29 (Hex/AcOEt, 4:6). IR (film) ν_{max} (cm^{-1}) 3028, 1722, 1697, 1650; ^1H NMR (500 MHz, $CDCl_3$) δ (ppm) 9.15 (brs, OH), 7.36−7.24 (m, 5H), 5.79 (dd, J = 10, 1.5 Hz, 1H), 5.72−5.69 (m, 1H), 4.53 (s, 2H), 3.45 (dd, J = 8.0, 3.5 Hz, 1H), 3.34 (dd, J = 8.5, 6.5 Hz, 1H), 3.01 (t, J = 10.5 Hz, 1H), 2.94 (brs, 1H), 2.80 (d, J = 19.0 Hz, 1H), 2.49−2.44 (m, 2H); ^{13}C NMR (125 MHz, $CDCl_3$) δ (ppm) 175.3, 174.7, 136.3, 128.9 (2C), 128.2, 128.1 (2C), 127.8, 125.3, 49.6, 47.1, 47.0, 36.5, 34.8, 28.2; HRMS (ESI+) for $C_{16}H_{17}NO_3Na$ (M + Na) calcd, 294.1106; found, 294.1096.

***rac*-(3a*S*,4*R*,5*S*,7a*R*)-2-Benzyl-5-methyl-3-oxo-2,3,3a,4,5,7a-hexahydro-1*H*-isoindole-4-carboxylic Acid (13f).** White solid. Yield: 51%. R_f = 0.46 (Hex/AcOEt, 3:7); ^1H NMR (400 MHz, $CDCl_3$) δ (ppm) 7.35−7.22 (m, 5H), 5.73 (d, J = 10.0 Hz, 1H), 5.61−5.59 (m, 1H), 4.51 (s, 2H), 3.32 (t, J = 8.4 Hz, 1H), 3.05 (d, J = 3.6 Hz, 1H), 3.02−2.97 (m, 2H), 2.88−2.81 (m, 1H), 2.42 (d, J = 12.8 Hz, 1H), 1.16 (d, J = 7.6 Hz, 3H); ^{13}C NMR (125 MHz, $CDCl_3$) δ (ppm) 175.9, 174.9, 136.4, 134.2, 128.9 (2C), 128.1 (2C), 127.7,

DOI: 10.1021/acs.jmedchem.5b01296
J. Med. Chem. XXXX, XXX, XXX−XXX

124.6, 49.5, 46.9, 44.4, 43.3, 34.6, 33.5, 22.0. Spectral data were consistent with data reported in the literature.[45]

***rac*-Benzyl ((3a*R*,7*R*,7a*S*)-7-Cyano-1-oxo-3,3a,7,7a-tetrahydro-1*H*-isoindol-2(6*H*)-yl)carbamate (9a).** Acid **13a** (170 mg, 0.51 mmol) was dissolved, under argon atmosphere, in THF (6.4 mL), then TEA (115 μL, 0.82 mmol) was added, and the reaction was cooled at −15 °C. Then, $EtCO_2Cl$ was added, and the reaction was stirred at −15 °C. After 15 min, a solution of NH_4OH (30% in water) was added, and the reaction was stirred 15 h at room temperature. The reaction was extracted 3 times with EtOAc. The organic phases were washed with water and brine, dried over Na_2SO_4, and concentrated under reduced pressure. The crude product was directly used in the next reaction step. To a cooled solution of the amide (21 mg, 0.064 mmol) in THF (1 mL) was added TEA (27 μL, 0.191 mmol). After stirring, TFAA (13.5 μL, 0.096 mmol) was added at 0 °C, and the reaction mixture was stirred for 1 h at 0 °C. Then, the reaction was quenched with water and extracted with $CHCl_3$ (3×). The organic phases were washed with water and brine, dried over Na_2SO_4, and concentrated under reduced pressure. The crude product was purified by flash chromatography (Hex/EtOAc 5:5), to give nitrile **9a** as a white solid (15 mg, 75%). R_f = 0.35 (1:1 Hex/AcOEt). IR (film) ν_{max} (cm^{-1}): 3278, 2923, 2241, 1754, 1738, 1711; ^1H NMR (300 MHz, $CDCl_3$) δ (ppm) 7.45−7.29 (m, 5H), 6.94 (bs, 1H), 5.92 (d, 1H, J = 9.8 Hz), 5.74−5.65 (m, 1H), 5.26−5.06 (m, 2H), 3.70−3.42 (m, 3H), 3.21−2.99 (m, 1H), 2.63−2.54 (m, 2H), 2.46 (bd, J = 9.4 Hz, 1H); ^{13}C NMR (75 MHz, $CDCl_3$) δ (ppm) 154.9, 135.3, 128.6 (2C), 128.5 (2C), 128.2, 126.0, 125.6, 119.4, 68.0, 51.9, 44.7, 33.5, 29.8, 23.6; HRMS (ESI +) for $C_{17}H_{17}N_3O_3Na$ (M + Na) calcd, 334.1162; found, 334.1160.

***rac*-Benzyl((4*R*,7a*R*)-3-oxo-4-(pyrrolidine-1-carbonyl)-1,3,3a,4,5,7a-hexahydro-2*H*-isoindol-2-yl)carbamate (15a).** Acid **13a** (100 mg, 0.304 mmol) was dissolved, under argon atmosphere, in DMF (3.5 mL). The solution was cooled to 0 °C, and TEA (212 μL, 1.52 mmol) was added followed by PivCl (55 μL, 0.455 mmol). After 1 h, pyrrolidine (124 μL, 1.52 mmol) was added, and the mixture was stirred overnight at room temperature. The reaction was quenched with H_2O and extracted with EtOAc, and the organic phases washed with 1 M HCl, saturated $NaHCO_3$, and brine, dried over Na_2SO_4, filtered, and concentrated under reduced pressure. The crude product was chromatographed on silica gel (Hex/EtOAc 2:8) to afford the product **15a** as a white solid (19 mg, 16%). R_f = 0.29 (AcOEt). IR (film) ν_{max} (cm^{-1}) 3211, 2970, 2876, 1744, 1715, 1617, 1454, 1228; ^1H NMR (500 MHz, $CDCl_3$) δ (ppm) 7.37−7.32 (m, 5H), 6.85 (brs, NH), 5.87 (d, J = 10.0 Hz, 1H), 5.71 (d, J = 10.0 Hz, 1H), 5.15 (brs, 2H), 4.06−4.01 (m, 1H), 3.57−3.53 (m, 2H), 3.42−3.39 (m, 4H), 2.50−2.46 (m, 1H), 2.35 (d, J = 20.0 Hz, 1H), 1.95−1.90 (m, 2H), 1.88−1.74 (m, 2H), 1.25 (brs, 2H); ^{13}C NMR (125 MHz, $CDCl_3$) δ (ppm) 172.1, 155.1, 135.6, 128.7, 128.5, 127.5, 125.9, 68.0, 52.6, 47.0, 46.6, 46.0, 33.3, 32.3, 29.8, 28.5, 26.3, 24.4; HRMS (ESI+) for $C_{21}H_{26}N_3O_4$ (M+ H) calcd, 384.1918; found, 384.1907.

***rac*-Benzyl((3a*S*,4*R*,5*S*,7a*R*)-5-methyl-3-oxo-4-(pyrrolidine-1-carbonyl)-1,3,3a,4,5,7a-hexahydro-2*H*-isoindol-2-yl)carbamate (15b).** Acid **13b** (150 mg, 0.435 mmol) was dissolved, under argon atmosphere, in DMF (4.2 mL). The solution was cooled to 0 °C, and TEA (304 μL, 2.177 mmol) was added followed by PivCl (75 μL, 0.610 mmol). After 1 h, pyrrolidine (193 μL, 2.177 mmol) was added, and the mixture was stirred overnight at room temperature. The reaction was quenched with H_2O, extracted with EtOAc, and the organic phases washed with 1 M HCl, saturated $NaHCO_3$, and brine, dried over Na_2SO_4, filtered, and concentrated under reduced pressure. The crude product was chromatographed on silica gel (Hex/EtOAc 75:25) to afford the product **15b** as a white solid (105 mg, 61%). R_f = 0.19 (Hex/EtOAc 2:8). IR (film) ν_{max} (cm^{-1}) 3209, 2958, 2872, 1743, 1715, 1617, 1453, 1230; ^1H NMR (500 MHz, $CDCl_3$) δ (ppm) 7.34−7.32 (m, 5H), 6.74 (brs, NH), 5.84 (d, J = 10.0 Hz, 1H), 5.61 (d, J = 10.0 Hz, 1H), 5.18−5.11 (m, 2H), 4.06−4.01 (m, 1H), 3.57−3.40 (m, 6H), 3.00 (d, J = 4.0 Hz, 1H), 2.57−2.56 (m, 1H), 2.42 (brs, 1H), 1.95−1.91 (m, 2H), 1.89−1.74 (m, 2H), 1.16 (d, J = 7.0 Hz, 3H); ^{13}C NMR (125 MHz, $CDCl_3$) δ (ppm) 173.8, 172.1, 155.2, 135.7, 133.8, 128.6, 128.4, 125.0, 67.7, 52.4, 47.0, 46.0, 44.3, 41.3, 33.9, 32.4, 26.2, 24.3, 22.4; HRMS (ESI+) for $C_{22}H_{28}N_3O_4$ (M+ H) calcd, 398.2074; found, 398.2068.

***rac*-*N*-((3a*S*,4*R*,7a*R*)-3-Oxo-4-(pyrrolidine-1-carbonyl)-1,3,3a,4,5,7a-hexahydro-2*H*-isoindol-2-yl)-2-phenylacetamide (15c).** Acid **13c** (200 mg, 0.636 mmol) was dissolved, under argon atmosphere, in DMF (6 mL). The solution was cooled to 0 °C, and TEA (443 μL, 3.18 mmol) was added followed by PivCl (110 μL, 0.890 mmol). After 1 h, pyrrolidine (282 μL, 3.18 mmol) was added, and the mixture was stirred overnight at room temperature. The reaction was quenched with H_2O, extracted with EtOAc, and the organic phases washed with 1 M HCl, saturated $NaHCO_3$, and brine, dried over Na_2SO_4, filtered, and concentrated under reduced pressure. The *exo* compound was selectively precipitated using ether and afforded the pure compound **15c** as a white solid (70 mg, 30%). R_f = 0.13 (EtOAc). IR (film) ν_{max} (cm^{-1}) 3232, 3026, 2974, 2874, 1729, 1686, 1613, 1454, 1348; ^1H NMR (400 MHz, $CDCl_3$) δ (ppm) 7.77 (brs, NH), 7.35−7.27 (m, 5H), 5.85 (d, J = 10.0 Hz, 1H), 5.70−5.67 (m, 1H), 3.99−3.93 (m, 1H), 3.60 (s, 2H), 3.49−3.34 (m, 6H), 2.53−2.46 (m, 2H), 2.31 (d, J = 18.4 Hz, 1H), 1.95−1.73 (m, 5H); ^{13}C NMR (125 MHz, $CDCl_3$) δ (ppm) 173.4, 172.3, 169.8, 133.9, 129.5 (2C), 129.1 (2C), 127.5, 127.3, 126.1, 52.4, 47.0, 46.4, 46.0, 41.5, 33.3, 32.5, 28.4, 26.3, 24.4; HRMS (ESI+) for $C_{21}H_{25}N_3O_3Na$ (M+ Na) calcd, 390.1788; found, 390.1790.

***rac*-(3a*R*,7*R*,7a*S*)-2-(Benzyloxy)-7-(pyrrolidine-1-carbonyl)-2,3,3a,6,7,7a-hexahydro-1*H*-isoindol-1-one (15d).** Acid **13d** (150 mg, 0.522 mmol) was dissolved, under argon atmosphere, in DMF (5 mL). The solution was cooled to 0 °C, and TEA (364 μL, 2.61 mmol) was added followed by PivCl (90 μL, 0.731 mmol). After 1 h, pyrrolidine (232 μL, 2.61 mmol) was added, and the mixture was stirred overnight at room temperature. The reaction was quenched with H_2O, extracted with EtOAc, and the organic phases washed with 1 M HCl, saturated $NaHCO_3$, brine, dried over Na_2SO_4, filtered, and concentrated under reduced pressure. The crude product was chromatographed on silica gel (Hex/EtOAc 2:8) to afford the product **15d** as a white solid (90 mg, 51%). R_f = 0.25 (Hex/EtOAc 2:8). IR (film) ν_{max} (cm^{-1}) 3480, 2951, 1705, 1634; ^1H NMR (400 MHz, $CDCl_3$) δ (ppm) 7.40−7.37 (m, 2H), 7.35−7.32 (m, 3H), 5.75−5.71 (m, 1H), 5.53−5.49 (m, 1H), 4.93 (q, J = 8.8 Hz, 2H), 3.55−3.37 (m, 5H), 3.15−3.09 (m, 2H), 2.95 (dd, J = 6.8, 2.4 Hz, 1H), 2.89 (dd, J = 6.4, 3.6 Hz, 1H), 2.25−2.19 (m, 1H), 2.15−2.11 (m, 1H), 1.97−1.90 (m, 2H), 1.88−1.79 (m, 2H); ^{13}C NMR (125 MHz, $CDCl_3$) δ (ppm) 172.6, 170.9, 135.2, 129.8 (2C), 129.0, 128.6 (2C), 127.3, 125.9, 76.9, 52.1, 46.8, 46.0, 39.9, 35.7, 29.2, 26.3, 24.3, 24.1; HRMS (ESI+) for $C_{20}H_{24}N_2O_3Na$ (M+ Na) calcd, 363.1679; found, 363.1688.

(3a*R*,7*R*,7a*S*)-2-Benzyl-7-(pyrrolidine-1-carbonyl)-2,3,3a,6,7,7a-hexahydro-1*H*-isoindol-1-one (15e). Acid **13e** (150 mg, 0.553 mmol) was dissolved, under argon atmosphere, in DMF (5.3 mL). The solution was cooled to 0 °C, and TEA (385 μL, 2.764 mmol) was added followed by PivCl (95 μL, 0.774 mmol). After 1 h, pyrrolidine (245 μL, 2.764 mmol) was added, and the mixture was stirred 15 h at room temperature. The reaction was quenched with H_2O, extracted with EtOAc, and the organic phases washed with 1 M HCl, saturated $NaHCO_3$, and brine, dried over Na_2SO_4, filtered, and concentrated under reduced pressure. The crude product was chromatographed on silica gel (Hex/EtOAc 2:8) to afford the product **15e** as a white solid (105 mg, 58%). R_f = 0.16 (Hex/EtOAc 2:8). IR (film) ν_{max} (cm^{-1}) 3211, 2970, 2876, 1744, 1715, 1617, 1454, 1228; ^1H NMR (400 MHz, $CDCl_3$) δ (ppm) 7.32−7.15 (m, 5H), 5.83 (dd, J = 9.6, 1.6 Hz, 1H), 5.69−5.65 (m,1H), 4.59 (d, J = 15.0 Hz, 1H), 4.27 (d, J = 15.0 Hz, 1H), 4.21−4.15 (m, 1H), 3.51−3.42 (m, 5H), 3.32−3.28 (m, 1H), 2.90 (dd, J = 10.8, 8.8 Hz, 1H), 2.50−2.40 (m, 1H), 2.36−2.32 (m, 2H), 2.03−1.75 (m, 4H); ^{13}C NMR (125 MHz, $CDCl_3$) δ (ppm) 173.7, 172.5, 136.8, 128.8 (2C), 128.1 (2C), 127.6, 127.5, 126.4, 49.7, 48.5, 47.1, 46.9, 45.9, 34.0, 33.7, 29.1, 26.4, 24.5; HRMS (ESI+) for $C_{20}H_{24}N_2O_2Na$ (M+ Na) calcd, 347.1730; found, 347.1737.

(3a*R*,6*S*,7*R*,7a*S*)-2-Benzyl-6-methyl-7-(pyrrolidine-1-carbonyl)-2,3,3a,6,7,7a-hexahydro-1*H*-isoindol-1-one (15f). Acid **13f** (200 mg, 0.70 mmol) was dissolved, under argon atmosphere, in DMF (6.7 mL). The solution was cooled to 0 °C, and TEA (488 μL, 3.50

DOI: 10.1021/acs.jmedchem.5b01296
J. Med. Chem. XXXX, XXX, XXX−XXX

mmol) was added followed by PivCl (121 μL, 0.98 mmol). After 1 h, pyrrolidine (311 μL, 3.50 mmol) was added, and the mixture was stirred 15 h at room temperature. The reaction was quenched with H_2O, extracted with EtOAc, and the organic phases washed with 1 M HCl, saturated $NaHCO_3$, and brine, dried over Na_2SO_4, filtered, and concentrated under reduced pressure. The crude product was chromatographed on silica gel (Hex/EtOAc 5:5) to afford the product **15f** as a white solid (168 mg, 71%). R_f = 0.34 (Hex/EtOAc 3:7). IR (film) υ_{max} (cm^{-1}) 2954, 2868, 1698, 1637, 1423, 1355, 1250; ^1H NMR (500 MHz, $CDCl_3$) δ (ppm) 7.32−7.29 (m, 2H), 7.26−7.23 (m, 1H), 7.20−7.18 (m, 2H), 5.79 (dt, *J* = 10.0, 1.5 Hz, 1H), 5.57 (dt, *J* = 10.0, 3.5 Hz, 1H), 4.62 (d, *J* = 15.0 Hz, 1H), 4.23 (d, *J* = 15.0 Hz, 1H), 4.19−4.14 (m, 1H), 3.54−3.43 (m, 4H), 3.29 (dd, *J* = 8.5, 7.5 Hz, 1H), 3.04 (d, *J* = 4.5 Hz, 1H), 2.89 (dt, *J* = 11.0, 8.5 Hz, 1H), 2.58−2.53 (m, 1H), 2.31 (dd, *J* = 13.0, 4.5 Hz, 1H), 2.01−1.76 (m, 4H), 1.14 (d, *J* = 7.0 Hz, 3H); ^{13}C NMR (125 MHz, $CDCl_3$) δ (ppm) 174.0, 172.3, 136.8, 133.8, 128.8 (2C), 128.1 (2C), 127.5, 125.5, 49.6, 47.1, 46.9, 46.1, 46.0, 41.6, 34.4, 34.2, 26.3, 24.4, 22.5; HRMS (ESI+) for $C_{21}H_{27}N_2O_2$ (M+ H) calcd, 339.2067; found, 339.2062.

Benzyl ((3a*S*,4*R*,7a*R*)-4-((*S*)-2-Cyanopyrrolidine-1-carbonyl)-3-oxo-1,3,3a,4,5,7a-hexahydro-2*H*-isoindol-2-yl)carbamate (7a) and Benzyl ((3a*R*,4*S*,7a*S*)-4-((*S*)-2-Cyanopyrrolidine-1-carbonyl)-3-oxo-1,3,3a,4,5,7a-hexahydro-2*H*-isoindol-2-yl)-carbamate (16a). Acid **13a** (189 mg, 0.572 mmol) was dissolved, under argon atmosphere, in DCM (4 mL). The solution was cooled to 0 °C, and TEA (400 μL, 2.86 mmol) was added followed by PivCl (70 μL, 0.572 mmol). After 1 h, a solution of (*S*)-cyano-pyrrolidine (184 mg, 0.686 mmol) and TEA (400 μL, 2.86 mmol) in DCM (2 mL) was added, and the solution was stirred overnight at room temperature. The reaction was quenched with H_2O, extracted with EtOAc, and the organic phases washed with 1 M HCl, saturated $NaHCO_3$, and brine, dried over Na_2SO_4, filtered, and concentrated under reduced pressure. The crude product was chromatographed on silica gel (Hex/EtOAc 2:8) to afford the products **7a** (20 mg) and **16a** (50 mg) as white solids (70 mg, 34%). IR (film) υ_{max} (cm^{-1}) 3269, 2980, 2956, 1742, 1714, 1651, 1431, 1312, 1232. Data for **7a**: R_f = 0.42 (EtOAc); ^1H NMR (500 MHz, $CDCl_3$): δ (ppm) 7.37−7.31 (m, 5H), 6.93 (brs, NH), 5.88 (d, *J* = 10.0 Hz, 1H), 5.72 (d, *J* = 10.0 Hz, 1H), 5.14 (brs, 2H), 4.67 (brs, 1H), 4.10−4.06 (m, 1H), 3.60−3.56 (m, 2H), 3.43−3.35 (m, 3H), 2.54−2.37 (m, 3H), 2.17−2.09 (m, 4H); ^{13}C NMR (125 MHz, $CDCl_3$): δ (ppm) 173.5, 172.8, 155.1, 135.5, 128.7 (3C), 128.6, 128.4, 127.2, 125.9, 118.7, 68.0, 52.6, 46.9, 46.6, 46.4, 33.2, 32.3, 30.1, 28.1, 25.3; HRMS (ESI+) for $C_{22}H_{24}N_4O_4Na$ (M+ Na) calcd, 431.1690; found, 431.1678. Data for **16a**: R_f = 0.46 (EtOAc); ^1H NMR (400 MHz, $CDCl_3$): δ (ppm) 7.38−7.31 (m, 5H), 6.87 (brs, 0.4NH), 6.69 (brs, 0.6NH), 5.87−5.84 (m, 1H), 5.80−5.70 (m, 1.6H), 5.20−5.11 (m, 2H), 4.68−4.66 (m, 0.5H), 4.52−4.47 (m, 0.5H), 3.66−3.54 (m, 1.7H), 3.51−3.34 (m, 3H), 3.30−3.14 (m, 1.3H), 2.86 (d, *J* = 10.0 Hz, 0.3H), 2.59−2.38 (m, 3H), 2.33−2.01 (m, 4.5H); ^{13}C NMR (125 MHz, $CDCl_3$): δ (ppm) 172.6, 172.4, 155.1, 154.9, 135.6, 135.4, 128.8, 128.7, 128.6, 128.4, 128.1, 127.5, 125.6, 124.9, 119.5, 118.6, 68.2, 68.0, 52.8, 52.5, 47.8, 47.1, 46.7, 46.7, 46.6, 46.2, 34.2, 33.9, 32.5, 32.3, 30.1, 28.6, 28.5, 25.5, 23.2; HRMS (ESI+) for $C_{22}H_{24}N_4O_4Na$ (M+ Na) calcd, 431.1690; found, 431.1684.

Benzyl ((3a*S*,4*R*,5*S*,7a*R*)-4-((*S*)-2-Cyanopyrrolidine-1-carbonyl)-5-methyl-3-oxo-1,3,3a,4,5,7a-hexahydro-2*H*-isoindol-2-yl)-carbamate (7b) and Benzyl ((3a*R*,4*S*,5*R*,7a*S*)-4-((*S*)-2-cyanopyrrolidine-1-carbonyl)-5-methyl-3-oxo-1,3,3a,4,5,7a-hexahydro-2*H*-isoindol-2-yl)carbamate (16b). Acid **13b** (212 mg, 0.616 mmol) was dissolved, under argon atmosphere, in DMF (4.1 mL). The solution was cooled to 0 °C, and BOP (381 mg, 0.862 mmol) was added, followed by (*S*)-cyano-pyrrolidine (264 mg, 0.985 mmol) and TEA (429 μL, 3.078 mmol). The mixture was stirred for 15 h at room temperature. The reaction was quenched with H_2O and extracted with EtOAc, and the organic layer was washed with 1 M HCl, saturated $NaHCO_3$, and brine, dried over Na_2SO_4, filtered, and evaporated. The crude product was chromatographed on silica gel (Hex/EtOAc 2:8) to afford the products **7b** (98 mg) and **16b** (68 mg) as white solids (166 mg, 64%). IR (film) υ_{max} (cm^{-1}) 3256, 2959, 2875, 1708, 1645, 1498, 1427, 1301, 1231. Data for **7b**: R_f = 0.58 (EtOAc); ^1H NMR (400 MHz, $CDCl_3$): δ (ppm) 7.38−7.31 (m, 5H), 6.73 (brs, NH), 5.86 (d, *J* = 9.6 Hz, 1H), 5.64−5.61 (m, 1H), 5.18−5.11 (m, 2H), 4.67 (brs, 1H), 4.12−4.06 (m, 1H), 3.65−3.55 (m, 2H), 3.48−3.36 (m, 2H), 2.95 (d, *J* = 4.4 Hz, 1H), 2.65−2.60 (m, 1H), 2.46−2.38 (m, 1H), 2.22−2.09 (m, 4H), 1.18 (d, *J* = 7.6 Hz, 3H); ^{13}C NMR (125 MHz, $CDCl_3$): δ (ppm) 173.8, 172.7, 155.1, 135.5, 133.7, 128.7 (3C), 128.6, 128.5, 125.0, 118.7, 68.0, 52.5, 46.9, 46.6, 44.3, 41.2, 33.7, 32.5, 30.0, 25.3, 22.4; HRMS (ESI+) for $C_{23}H_{26}N_4O_4Na$ (M+ Na) calcd, 445.1846; found, 445.1836. Data for **16b**: R_f = 0.70 (EtOAc); ^1H NMR (400 MHz, $CDCl_3$): δ (ppm) 7.37−7.33 (m, 5H), 6.85 (brs, 0.4NH), 6.66 (brs, 0.6NH), 5.84 (d, *J* = 10.0 Hz, 1H), 5.73 (dd, *J* = 7.6, 1.2 Hz, 0.5H), 5.70−5.61 (m, 1H), 5.21−5.11 (m, 2H), 4.67−4.65 (m, 0.5H), 4.50−4.46 (m, 0.5H), 3.66−3.14 (m, 5H), 3.12−3.03 (m, 1H), 2.70−2.67 (m, 0.5H), 2.59−2.53 (m, 1H), 2.33−2.02 (m, 4H), 1.22−1.13 (m, 3H); ^{13}C NMR (125 MHz, $CDCl_3$): δ (ppm) 172.5, 172.4, 155.2, 154.9, 135.4, 134.5, 133.8, 128.8 (2C), 128.7 (2C), 128.4, 124.8, 124.2, 119.6, 118.5, 68.3, 68.1, 52.8, 52.5, 47.9, 46.7, 46.2, 42.0, 41.6, 34.1, 33.9, 32.6, 32.4, 32.2, 30.2, 25.5, 23.3, 22.1, 21.9; HRMS (ESI+) for $C_{23}H_{26}N_4O_4Na$ (M+ Na) calcd, 445.1846; found, 445.1839.

***N*-((3a*S*,4*R*,7a*R*)-4-((*S*)-2-Cyanopyrrolidine-1-carbonyl)-3-oxo-1,3,3a,4,5,7a-hexahydro-2*H*-isoindol-2-yl)-2-phenylacetamide (7c) and *N*-((3a*R*,4*S*,7a*S*)-4-((*S*)-2-Cyanopyrrolidine-1-carbonyl)-3-oxo-1,3,3a,4,5,7a-hexahydro-2*H*-isoindol-2-yl)-2-phenylacetamide (16c).** The acid **13c** (700 mg, 2.23 mmol) was dissolved, under argon atmosphere, in DMF (15 mL). The solution was cooled to 0 °C, and BOP (1.38 g, 3.12 mmol) was added, followed by (*S*)-cyano-pyrrolidine (956 mg, 3.56 mmol) and TEA (1.5 mL, 11.13 mmol). The mixture was stirred 15 h at room temperature. The reaction was quenched with H_2O, extracted with EtOAc, and the organic layer was washed with 1 M HCl, saturated $NaHCO_3$, and brine, dried over Na_2SO_4, filtered, and evaporated. The crude product was chromatographed on silica gel (Hex/EtOAc 2:8 to EtOAc/MeOH 8:2) to afford the products **7c** (70 mg) and **16c** (59 mg) as white solids (129 mg, 15%). IR (film) υ_{max} (cm^{-1}) 3271, 3027, 2926, 1727, 1680, 1649, 1428, 1345, 1188. Data for **7c**: R_f = 0.15 (AcOEt); ^1H NMR (500 MHz, $CDCl_3$): δ (ppm) 7.37−7.29 (m, 5H), 5.88 (dd, *J* = 9.6, 1.2 Hz, 1H), 5.73−5.69 (m, 1H), 4.68−4.65 (m, 1H), 4.06−4.00 (m, 1H), 3.64−3.59 (m, 3H), 3.49−3.32 (m, 4H), 2.57−2.49 (m, 2H), 2.38 (d, *J* = 18.0 Hz, 1H), 2.23−2.08 (m, 4H); ^{13}C NMR (125 MHz, $CDCl_3$): δ (ppm) 173.1, 172.9, 169.7, 133.6, 129.5 (2C), 129.2 (2C), 127.8, 127.1, 126.0, 118.7, 52.5, 46.9, 46.5, 46.2, 41.7, 33.2, 32.4, 30.1, 28.0, 25.4; HRMS (ESI+) for $C_{22}H_{25}N_4O_3$ (M + H) calcd, 393.1921; found, 393.1924. Data for **16c**: R_f = 0.25 (EtOAc); ^1H NMR (500 MHz, $CDCl_3$): δ (ppm) 8.04 (brs, 0.5NH), 7.66 (brs, 0.5NH), 7.35−7.28 (m, 5H), 5.83 (td, *J* = 11.0, 1.0 Hz, 1H), 5.76−5.73 (m, 1H), 5.70−5.67 (m, 0.5H), 4.63 (d, *J* = 5.5 Hz, 0.5H), 4.38 (t, *J* = 7.0 Hz, 0.5H), 3.60−3.56 (m, 2.5H), 3.51−3.32 (m, 4H), 3.28−3.22 (m, 0.5H), 3.16−3.10 (m, 0.5H), 2.60 (td, *J* = 13.0, 5.0 Hz, 1H), 2.50−2.42 (m, 1H), 2.33−2.00 (m, 5H); ^{13}C NMR (125 MHz, $CDCl_3$): δ (ppm) 173.4, 172.9 (2C), 172.5, 169.9, 169.6, 133.9, 133.7, 129.5 (2C), 129.4 (2C), 129.1 (2C), 129.0 (2C), 127.9, 127.6, 127.5, 127.1, 125.8, 125.0, 119.4, 118.7, 52.6, 52.3, 47.7, 47.0, 46.7, 46.6, 46.3, 46.1, 41.4, 41.2, 34.1, 33.7, 32.5, 32.4, 32.2, 30.1, 28.5, 28.3, 25.4, 23.1; HRMS (ESI+) for $C_{22}H_{25}N_4O_3$ (M + H) calcd, 393.1921; found, 393.1934.

(*S*)-1-((3a*S*,4*R*,7a*R*)-2-(Benzyloxy)-3-oxo-2,3,3a,4,5,7a-hexahydro-1*H*-isoindole-4-carbonyl)pyrrolidine-2-carbonitrile (7d) and (*S*)-1-((3a*R*,4*S*,7a*S*)-2-(Benzyloxy)-3-oxo-2,3,3a,4,5,7a-hexahydro-1*H*-isoindole-4-carbonyl)pyrrolidine-2-carbonitrile (16d). Acid **13d** (215 mg, 0.748 mmol) was dissolved, under argon atmosphere, in DMF (5 mL). The solution was cooled to 0 °C, and BOP (463 mg, 1.047 mmol) was added, followed by (*S*)-cyano-pyrrolidine (321 mg, 1.197 mmol) and TEA (521 μL, 3.741 mmol). The mixture was stirred for 15 h at room temperature. The reaction was quenched with H_2O, extracted with EtOAc, and the organic layer was washed with 1 M HCl, saturated $NaHCO_3$, and brine, dried over Na_2SO_4, filtered, and evaporated. The crude product was chromatographed on silica gel (Hex/EtOAc 2:8) to afford the products **7d** (100 mg) and **16d** (80 mg) as white solids (180 mg, 66%). IR (film) υ_{max} (cm^{-1}) 2926, 2880, 2238, 1708, 1648. Data for **7d**: R_f = 0.25 (AcOEt); ^1H NMR (400 MHz, $CDCl_3$): δ (ppm) 7.42−7.36 (m, 5H), 5.78 (dd,

DOI: 10.1021/acs.jmedchem.5b01296
J. Med. Chem. XXXX, XXX, XXX−XXX

J = 10.0, 2.0 Hz, 1H), 5.71−5.66 (m, 1H), 4.98−4.89 (m, 2H), 4.71−4.68 (m, 1H), 4.19−4.13 (m, 1H), 3.65−3.59 (m, 1H), 3.41 (t, J = 7.2 Hz, 1H), 3.36−3.33 (m, 1H), 3.31−3.23 (m, 1H), 3.01 (dd, J = 10.8, 7.2 Hz, 1H), 2.52−2.36 (m, 2H), 2.27−2.09 (m, 5H); ^{13}C NMR (125 MHz, $CDCl_3$): δ (ppm) 172.7, 169.7, 135.3, 129.7 (2C), 129.0, 128.7 (2C), 127.3, 125.6, 118.7, 77.4, 51.2, 46.9, 46.6, 46.1, 33.2, 31.5, 30.1, 28.2, 25.3; HRMS (ESI+) for $C_{21}H_{23}N_3O_3Na$ (M + Na) calcd, 388.1630; found, 388.1641. Data for **16d**: R_f = 0.33 (Hex/EtOAc 2:8); ^{1}H NMR (400 MHz, $CDCl_3$): δ (ppm) 7.45−7.34 (m, 5H), 5.88 (d, J = 6.8 Hz, 0.5H), 5.76−5.67 (m, 2H), 5.00−4.87 (m, 2H), 4.74 (dd, J = 7.2, 2.0 Hz, 0.5H), 4.62 (td, J = 8.8, 2.0 Hz, 0.5H), 3.68−3.62 (m, 0.5H), 3.48−3.34 (m, 2.5H), 3.19−3.13 (m, 0.5H), 3.05−2.97 (m, 2H), 2.46−2.03 (m, 7H); ^{13}C NMR (125 MHz, $CDCl_3$): δ (ppm) 172.6, 172.3, 169.7, 169.5, 135.5, 135.1, 129.9 (2C), 129.7 (2C), 129.1, 129.0, 128.8 (2C), 128.7 (2C), 128.0, 127.5, 125.4, 124.7, 119.6, 118.6, 77.9, 51.4, 51.1, 47.7, 47.2, 46.7, 46.5, 46.4, 46.1, 34.3, 34.1, 32.3, 31.8, 31.1, 30.2, 28.6, 28.6, 25.6, 23.1; HRMS (ESI+) for $C_{21}H_{23}N_3O_3Na$ (M + Na) calcd, 388.1632; found, 388.1634.

(*S*)-1-((3a*S*,4*R*,7a*R*)-2-Benzyl-3-oxo-2,3,3a,4,5,7a-hexahydro-1*H*-isoindole-4-carbonyl)pyrrolidine-2-carbonitrile (7e) and (*S*)-1-((3a*R*,4*S*,7a*S*)-2-Benzyl-3-oxo-2,3,3a,4,5,7a-hexahydro-1*H*-isoindole-4-carbonyl)pyrrolidine-2-carbonitrile (16e). Acid **13e** (158 mg, 0.582 mmol) was dissolved, under argon atmosphere, in DMF (6 mL). The solution was cooled to 0 °C, and BOP (360 mg, 0.815 mmol) was added, followed by (*S*)-cyano-pyrrolidine (250 mg, 0.932 mmol) and TEA (406 μL, 2.910 mmol). The mixture was stirred 15 h at room temperature. The reaction was quenched with H_2O and extracted with EtOAc, and the organic layer was washed with 1 M HCl, saturated $NaHCO_3$, and brine, dried over Na_2SO_4, filtered, and evaporated. The crude product was chromatographed on silica gel with eluent (Hex/EtOAc 3:7) to afford the products **7e** (43 mg) and **16e** (20 mg) as white solids (63 mg, 31%). IR (film) υ_{max} (cm-1) 3476, 2968, 2043, 1689, 1632. Data for **7e**: R_f = 0.28 (AcOEt); ^{1}H NMR (500 MHz, $CDCl_3$): δ (ppm) 7.36−7.28 (m, 3H), 7.22−7.20 (m, 2H), 5.89−5.86 (m, 1H), 5.74−5.70 (m, 1H), 4.79−4.77 (m, 1H), 4.60 (d, J = 14.5 Hz, 1H), 4.31−4.25 (m, 2H), 3.71−3.67 (m, 1H), 3.47−3.39 (m, 2H), 3.35 (dd, J = 9.0, 7.5 Hz, 1H), 2.97 (dd, J = 11.0, 8.5 Hz, 1H), 2.56−2.49 (m, 1H), 2.46−2.44 (m, 1H), 2.40 (dd, J = 12.5, 4.5 Hz, 1H), 2.29−2.16 (m, 4H); ^{13}C NMR (125 MHz, $CDCl_3$): δ (ppm) 173.5, 173.2, 136.6, 128.9 (2C), 128.0 (2C), 127.7, 127.3, 126.3, 118.8, 49.8, 48.3, 47.0, 46.9, 46.6, 34.1, 33.6, 30.2, 28.6, 25.4; HRMS (ESI+) for $C_{21}H_{23}N_3O_2Na$ (M + Na) calcd, 372.1682; found, 372.1681. Data for **16e**: R_f = 0.44 (Hex/EtOAc 2:8); ^{1}H NMR (400 MHz, $CDCl_3$): δ (ppm) 7.33−7.24 (m, 3H), 7.20−7.14 (m, 2H), 6.07 (dd, J = 7.2, 1.6 Hz, 0.5H), 5.84−5.80 (m, 1H), 5.76−5.67 (m, 1H), 4.77−4.71 (m, 0.5H), 4.55 (dd, J = 15.2, 6.4 Hz, 1H), 4.35 (d, J = 15.2 Hz, 0.5H), 4.24 (d, J = 14.8 Hz, 0.5H), 3.70−3.64 (m, 0.5H), 3.55−3.52 (m, 0.5H), 3.49−3.40 (m, 2H), 3.35−3.30 (m, 1H), 3.23−3.08 (m, 1H), 3.00−2.92 (m, 1H), 2.50−2.47 (m, 2H), 2.40−2.22 (m, 3H), 2.18−2.05 (m, 2H); ^{13}C NMR (125 MHz, $CDCl_3$): δ (ppm) 173.6, 172.9, 172.8, 136.5, 136.4, 129.0, 128.9 (2C), 128.1, 128.0 (2C), 127.9, 127.8, 127.7, 127.6, 126.1, 125.4, 119.7, 118.6, 49.9, 49.4, 48.6, 48.6, 47.8, 47.2, 47.0, 46.8, 46.7, 46.2, 34.8, 34.5, 34.3, 34.2, 32.3, 30.2, 29.2, 29.0, 25.6, 23.2; HRMS (ESI+) for $C_{21}H_{23}N_3O_2Na$ (M + Na) calcd, 372.1682; found, 372.1692.

(*S*)-1-((3a*S*,4*R*,5*S*,7a*R*)-2-Benzyl-5-methyl-3-oxo-2,3,3a,4,5,7a-hexahydro-1*H*-isoindole-4-carbonyl)pyrrolidine-2-carbonitrile (7f) and (*S*)-1-((3a*R*,4*S*,5*R*,7a*S*)-2-Benzyl-5-methyl-3-oxo-2,3,3a,4,5,7a-hexahydro-1*H*-isoindole-4-carbonyl)-pyrrolidine-2-carbonitrile (16f). Acid **13f** (300 mg, 1.051 mmol) was dissolved, under argon atmosphere, in DMF (7 mL). The solution was cooled to 0 °C, and BOP (651 mg, 1.471 mmol) was added, followed by (*S*)-cyano-pyrrolidine (451 mg, 1.680 mmol) and TEA (733 μL, 5.256 mmol). The mixture was stirred 15 h at room temperature. The reaction was quenched with H_2O, extracted with EtOAc, and the organic layer was washed with 1 M HCl, saturated $NaHCO_3$, and brine, dried over Na_2SO_4, filtered, and evaporated. The crude product was chromatographed on silica gel (Hex/EtOAc 4:6) to afford the products **7f** (120 mg) and **16f** (159 mg) as white solids (279 mg, 73%). IR (film) υ_{max} (cm^{-1}) 3027, 2960, 2873, 1690, 1647, 1425, 1351. Data for **7f**: R_f = 0.54 (AcOEt); ^{1}H NMR (400 MHz, $CDCl_3$): δ (ppm) 7.34−7.27 (m, 3H), 7.19−7.17 (m, 2H), 5.82 (dt, J = 10.0, 2.0 Hz, 1H), 5.59 (dt, J = 10.0, 2.8 Hz, 1H), 4.76−4.74 (m, 1H), 4.59 (d, J = 14.8 Hz, 1H), 4.27−4.20 (m, 2H), 3.69−3.65 (m, 1H), 3.43−3.30 (m, 2H), 2.99 (d, J = 4.8 Hz, 1H), 2.93 (dd, J = 10.8, 8.8 Hz, 1H), 2.67−2.59 (m, 1H), 2.34 (dd, J = 12.4, 4.8 Hz, 1H), 2.27−2.14 (m, 4H), 1.18 (d, J = 7.2 Hz, 3H); ^{13}C NMR (125 MHz, $CDCl_3$): δ (ppm) 173.7, 173.1, 136.6, 133.7, 128.9 (2C), 128.0 (2C), 127.7, 125.4, 118.9, 49.7, 47.0, 47.0, 46.6, 46.1, 41.5, 34.3, 34.1, 30.2, 25.4, 22.5; HRMS (ESI+) for $C_{22}H_{26}N_3O_2$ (M + H) calcd, 364.2019; found, 364.2015. Data for **16f**: R_f = 0.63 (EtOAc); ^{1}H NMR (500 MHz, $CDCl_3$): δ (ppm) 7.33−7.25 (m, 3H), 7.20−7.15 (m, 2H), 5.99 (dd, J = 7.5, 1.5 Hz, 0.6H), 5.79 (dt, J = 10.0, 2.0 Hz, 1H), 5.65−5.59 (m, 1H), 4.73−4.70 (m, 0.6H), 4.58 (d, J = 15.0 Hz, 0.6H), 4.52 (d, J = 15.0 Hz, 0.4H), 4.36 (d, J = 15.0 Hz, 0.4H), 4.22 (d, J = 15.0 Hz, 0.6H), 3.68−3.64 (m, 0.6H), 3.49−3.39 (m, 1H), 3.34−3.30 (m, 1H), 3.20−3.07 (m, 2H), 2.98−2.92 (m, 1H), 2.71−2.66 (m, 0.6H), 2.61−2.57 (m, 0.4H), 2.43 (dd, J = 13.0, 5.0 Hz, 1H), 2.37−2.25 (m, 2H), 2.18−2.05 (m, 2H), 1.20 (d, J = 7.5 Hz, 1.6H), 1.16−1.08 (m, 1.4H); ^{13}C NMR (125 MHz, $CDCl_3$): δ (ppm) 173.9, 173.2, 172.8, 136.5, 136.4, 134.4, 133.8, 128.9 (2C), 128.9 (2C), 128.0 (2C), 128.0 (2C), 127.9, 119.9, 118.6, 49.8, 49.3, 47.9, 47.2, 47.1, 46.8, 46.7, 46.4, 46.2, 45.9, 42.5, 42.1, 34.5, 34.4, 34.4, 34.3, 32.3, 30.2, 25.6, 23.3, 22.1, 22.0; HRMS (ESI+) for $C_{22}H_{25}N_3O_2Na$ (M + Na) calcd, 386.1839; found, 386.1822.

■ ASSOCIATED CONTENT

Supporting Information

The Supporting Information is available free of charge on the ACS Publications website at DOI: 10.1021/acs.jmedchem.5b01296.

Experimental details (PDF)

Crystallographic data (CSV)

■ AUTHOR INFORMATION

Corresponding Author

*Phone: 514-398-8543. Fax: 514-398-3797. E-mail, nicolas.moitessier@mcgill.ca.

Notes

The authors declare no competing financial interest.

■ ACKNOWLEDGMENTS

We thank CIHR for funding (operating grant). S.D.C. thanks FQRNT for a scholarship. Natural Sciences and Engineering Research Council of Canada (NSERC) for a grant to K.A., and the FRQNT Center in Green Chemistry and Catalysis (CGCC) at McGill University (Canada).

■ ABBREVIATIONS USED

BOP, benzotriazol-1-yl-oxy-tris(dimethylamino)-phosphonium-hexafluorophosphate; CNS, central nervous system; DCM, dichloromethane; DMF, dimethylformamide; Piv, pivaloyl; POP, prolyl oligopeptidase; TEA, trimethylamine; TFAA, trifluoroacetic anhydride; THF, tetrahydrofuran

■ REFERENCES

(1) Lawandi, J.; Gerber-Lemaire, S.; Juillerat-Jeanneret, L.; Moitessier, N. Inhibitors of prolyl oligopeptidases for the therapy of human diseases: Defining diseases and inhibitors. *J. Med. Chem.* **2010**, *53*, 3423−3438.

(2) Lambeir, A. M. Translational research on prolyl oligopeptidase inhibitors: The long road ahead. *Expert Opin. Ther. Pat.* **2011**, *21*, 977−981.

DOI: 10.1021/acs.jmedchem.5b01296
J. Med. Chem. XXXX, XXX, XXX−XXX

(3) López, A.; Tarragó, T.; Giralt, E. Low molecular weight inhibitors of Prolyl Oligopeptidase: A review of compounds patented from 2003 to 2010. *Expert Opin. Ther. Pat.* **2011**, *21*, 1023−1044.
(4) Cunningham, D. F.; O'Connor, B. Identification and initial characterisation of a N-benzyloxycarbonyl-prolyl-prolinal (Z-Pro-prolinal)-insensitive 7-(N-benzyloxycarbonyl-glycyl-prolyl-amido)-4-methylcoumarin (Z-Gly-Bro-NH-Mec)-hydrolysing peptidase in bovine serum. *Eur. J. Biochem.* **1997**, *244*, 900−903.
(5) Toide, K.; Shinoda, M.; Iwamoto, Y.; Fujiwara, T.; Okamiya, K.; Uemura, A. A novel propyl endopeptidase inhibitor, JTP-4819, with potential for treating Alzheimer's disease. *Behav. Brain Res.* **1997**, *83*, 147−151.
(6) Jarho, E. M.; Venäläinen, J. I.; Huuskonen, J.; Christiaans, J. A. M.; Garcia-Horsman, J. A.; Forsberg, M. M.; Jarvinen, T.; Gynther, J.; Männistö, P. T.; Wallén, E. A. A. A cyclopent-2-enecarbonyl group mimics proline at the P2 position of prolyl oligopeptidase inhibitors. *J. Med. Chem.* **2004**, *47*, 5605−5607.
(7) Jalkanen, A. J.; Hakkarainen, J. J.; Lehtonen, M.; Venäläinen, T.; Kääriäinen, T. M.; Jarho, E.; Suhonen, M.; Forsberg, M. M. Brain pharmacokinetics of two prolyl oligopeptidase inhibitors, JTP-4819 and KYP-2047, in the rat. *Basic Clin. Pharmacol. Toxicol.* **2011**, *109*, 443−451.
(8) Venäläinen, J. I.; Garcia-Horsman, J. A.; Forsberg, M. M.; Jalkanen, A.; Wallén, E. A. A.; Jarho, E. M.; Christiaans, J. A. M.; Gynther, J.; Männistö, P. T. Binding kinetics and duration of in vivo action of novel prolyl oligopeptidase inhibitors. *Biochem. Pharmacol.* **2006**, *71*, 683−692.
(9) Barelli, H.; Petit, A.; Hirsch, E.; Wilk, S.; De Nanteuil, G.; Morain, P.; Checler, F. S 17092−1, a highly potent, specific and cell permeant inhibitor of human proline endopeptidase. *Biochem. Biophys. Res. Commun.* **1999**, *257*, 657−661.
(10) Van Der Veken, P.; Fülöp, V.; Rea, D.; Gerard, M.; Van Elzen, R.; Joossens, J.; Cheng, J. D.; Baekelandt, V.; De Meester, I.; Lambeir, A. M.; Augustyns, K. P2-substituted N-acylprolylpyrrolidine inhibitors of prolyl oligopeptidase: Biochemical evaluation, binding mode determination, and assessment in a cellular model of synucleinopathy. *J. Med. Chem.* **2012**, *55*, 9856−9867.
(11) Lambeir, A. M. Interaction of prolyl oligopeptidase with α-synuclein. *CNS Neurol. Disord.: Drug Targets* **2011**, *10*, 349−354.
(12) Myöhänen, T. T.; Hannula, M. J.; Van Elzen, R.; Gerard, M.; Van Der Veken, P.; García-Horsman, J. A.; Baekelandt, V.; Männistö, P. T.; Lambeir, A. M. A prolyl oligopeptidase inhibitor, KYP-2047, reduces α-synuclein protein levels and aggregates in cellular and animal models of Parkinson's disease. *Br. J. Pharmacol.* **2012**, *166*, 1097−1113.
(13) Hannula, M. J.; Myöhänen, T. T.; Tenorio-Laranga, J.; Männistö, P. T.; Garcia-Horsman, J. A. Prolyl oligopeptidase colocalizes with α-synuclein, β-amyloid, tau protein and astroglia in the post-mortem brain samples with Parkinson's and Alzheimer's diseases. *Neuroscience* **2013**, *242*, 140−150.
(14) Lawandi, J.; Toumieux, S.; Seyer, V.; Campbell, P.; Thielges, S.; Juillerat-Jeanneret, L.; Moitessier, N. Constrained peptidomimetics reveal detailed geometric requirements of covalent prolyl oligopeptidase inhibitors. *J. Med. Chem.* **2009**, *52*, 6672−6684.
(15) De Cesco, S.; Deslandes, S.; Therrien, E.; Levan, D.; Cueto, M.; Schmidt, R.; Cantin, L. D.; Mittermaier, A.; Juillerat-Jeanneret, L.; Moitessier, N. Virtual screening and computational optimization for the discovery of covalent prolyl oligopeptidase inhibitors with activity in human cells. *J. Med. Chem.* **2012**, *55*, 6306−6315.
(16) Lawandi, J.; Toumieux, S.; Seyer, V.; Campbell, P.; Thielges, S.; Juillerat-Jeanneret, L.; Moitessier, N. Constrained peptidomimetics reveal detailed geometric requirements of covalent prolyl oligopeptidase inhibitors. *J. Med. Chem.* **2009**, *52*, 6672−6684.
(17) Johnson, D. S.; Weerapana, E.; Cravatt, B. F. Strategies for discovering and derisking covalent, irreversible enzyme inhibitors. *Future Med. Chem.* **2010**, *2*, 949−964.
(18) Zhou, S.; Chan, E.; Duan, W.; Huang, M.; Chen, Y. Z. Drug bioactivation, covalent binding to target proteins and toxicity relevance. *Drug Metab. Rev.* **2005**, *37*, 41−213.
(19) Guterman, L. Covalent Drugs Form Long-Lived Ties. *Chem. Eng. News* **2011**, *89*, 19−26.
(20) Kalgutkar, A. S.; Dalvie, D. K. Drug discovery for a new generation of covalent drugs. *Expert Opin. Drug Discovery* **2012**, *7*, 561−581.
(21) Robertson, J. G. Mechanistic basis of enzyme-targeted drugs. *Biochemistry* **2005**, *44*, 5561−5571.
(22) Singh, J.; Petter, R. C.; Baillie, T. A.; Whitty, A. The resurgence of covalent drugs. *Nat. Rev. Drug Discovery* **2011**, *10*, 307−317.
(23) Potashman, M. H.; Duggan, M. E. Covalent modifiers: An orthogonal approach to drug design. *J. Med. Chem.* **2009**, *52*, 1231−1246.
(24) Smith, A. J. T.; Zhang, X.; Leach, A. G.; Houk, K. N. Beyond picomolar affinities: Quantitative aspects of noncovalent and covalent binding of drugs to proteins. *J. Med. Chem.* **2009**, *52*, 225−233.
(25) Fleming, F. F.; Yao, L.; Ravikumar, P. C.; Funk, L.; Shook, B. C. Nitrile-containing pharmaceuticals: Efficacious roles of the nitrile pharmacophore. *J. Med. Chem.* **2010**, *53*, 7902−7917.
(26) Huot, M.; Moitessier, N. Expedient synthesis of novel bicyclic peptidomimetic scaffolds. *Tetrahedron Lett.* **2010**, *51*, 2820−2823.
(27) Szeltner, Z.; Rea, D.; Renner, V.; Fülöp, V.; Polgár, L. Electrostatic effects and binding determinants in the catalysis of prolyl oligopeptidase: Site-specific mutagenesis at the oxyanion binding site. *J. Biol. Chem.* **2002**, *277*, 42613−42622.
(28) Therrien, E.; Weill, N.; Tomberg, A.; Corbeil, C. R.; Lee, D.; Moitessier, N. Docking ligands into flexible and solvated macromolecules. 7. Impact of protein flexibility and water molecules on docking-based virtual screening accuracy. *J. Chem. Inf. Model.* **2014**, *54*, 3198−3210.
(29) Racys, D. T.; Rea, D.; Fülöp, V.; Wills, M. Inhibition of prolyl oligopeptidase with a synthetic unnatural dipeptide. *Bioorg. Med. Chem.* **2010**, *18*, 4775−4782.
(30) Singh, T.; Biswas, D.; Jayaram, B. AADS - An automated active site identification, docking, and scoring protocol for protein targets based on physicochemical descriptors. *J. Chem. Inf. Model.* **2011**, *51*, 2515−2527.
(31) Tomberg, A.; De Cesco, S.; Huot, M.; Moitessier, N. Solvent effect in diastereoselective intramolecular Diels−Alder reactions. *Tetrahedron Lett.* **2015**, *56*, 6852−6856.
(32) Nguyen, L. A.; He, H.; Pham-Huy, C. Chiral drugs: An overview. *Int. J. Biomed. Sci.* **2006**, *2*, 85−100.
(33) Morrison, J. F. Kinetics of the reversible inhibition of enzyme-catalysed reactions by tight-binding inhibitors. *Biochim. Biophys. Acta* **1969**, *185*, 269−286.
(34) Schiavini, P.; Pottel, J.; Moitessier, N.; Auclair, K. Metabolic instability of cyanothiazolidine-based prolyl oligopeptidase inhibitors: A structural assignment challenge and potential medicinal chemistry implications. *ChemMedChem* **2015**, *10*, 1174−1183.
(35) Wong, Y. C.; Qian, S.; Zuo, Z. Regioselective biotransformation of CNS drugs and its clinical impact on adverse drug reactions. *Expert Opin. Drug Metab. Toxicol.* **2012**, *8*, 833−854.
(36) Kalgutkar, A. S.; Gardner, I.; Obach, R. S.; Shaffer, C. L.; Callegari, E.; Henne, K. R.; Mutlib, A. E.; Dalvie, D. K.; Lee, J. S.; Nakai, Y.; O'Donnell, J. P.; Boer, J.; Harriman, S. P. A comprehensive listing of bioactivation pathways of organic functional groups. *Curr. Drug Metab.* **2005**, *6*, 161−225.
(37) Stepan, A. F.; Walker, D. P.; Bauman, J.; Price, D. A.; Baillie, T. A.; Kalgutkar, A. S.; Aleo, M. D. Structural alert/reactive metabolite concept as applied in medicinal chemistry to mitigate the risk of idiosyncratic drug toxicity: A perspective based on the critical examination of trends in the top 200 drugs marketed in the United States. *Chem. Res. Toxicol.* **2011**, *24*, 1345−1410.
(38) Gill, S. C.; von Hippel, P. H. Calculation of protein extinction coefficients from amino acid sequence data. *Anal. Biochem.* **1989**, *182*, 319−326.
(39) Morrison, J. F. Kinetics of the reversible inhibition of enzyme-catalysed reactions by tight-binding inhibitors. *Biochimica et Biophysica Acta (BBA) - Enzymology* **1969**, *185*, 269−286.

DOI: 10.1021/acs.jmedchem.5b01296
J. Med. Chem. XXXX, XXX, XXX−XXX

(40) Corbeil, C. R.; Englebienne, P.; Moitessier, N. Docking ligands into flexible and solvated macromolecules. 1. Development and validation of FITTED 1.0. *J. Chem. Inf. Model.* **2007**, *47*, 435−449.
(41) Therrien, E.; Englebienne, P.; Arrowsmith, A. G.; Mendoza-Sanchez, R.; Corbeil, C. R.; Weill, N.; Campagna-Slater, V.; Moitessier, N. Integrating medicinal chemistry, organic/combinatorial chemistry, and computational chemistry for the discovery of selective estrogen receptor modulatorswith FORECASTER, a novel platform for drug discovery. *J. Chem. Inf. Model.* **2012**, *52*, 210−224.
(42) Sheldrick, G. M. A short history of SHELX. *Acta Crystallogr., Sect. A: Found. Crystallogr.* **2008**, *64*, 112−122.
(43) Farrugia, L. J. WinGX suite for small-molecule single-crystal crystallography. *J. Appl. Crystallogr.* **1999**, *32*, 837−838.
(44) Gulías, M.; Durán, J.; López, F.; Castedo, L.; Mascareñas, J. L. Palladium-Catalyzed [4 + 3] Intramolecular Cycloaddition of Alkylidenecyclopropanes and Dienes. *J. Am. Chem. Soc.* **2007**, *129*, 11026−11027.
(45) Mellor, J. M.; Wagland, A. M. Synthesis of hydroisoindoles via intramolecular Diels-Alder reactions of functionalised amido trienes. *J. Chem. Soc., Perkin Trans. 1* **1989**, 997−1005.

DOI: 10.1021/acs.jmedchem.5b01296
J. Med. Chem. XXXX, XXX, XXX−XXX